University of Glasgow

DEPARTMENT OF

AEROSPACE ENGINEERING

A Fast Computational Module for the Calculation of Equilibrium State Variables and Sonic Speeds in Chemically Reacting Air, for Applications in CFD.

by

J. M. Anderson

G. U. Aero. Reoprt No. 9206 February 1992

A Fast Computational Module for the Calculation of Equilibrium State Variables and Sonic Speeds in Chemically Reacting Air, for Applications in CFD.

by

J. M. Anderson

G. U. Aero. Reoprt No. 9206 February 1992

A FAST COMPUTATIONAL MODULE FOR THE CALCULATION OF EQUILIBRIUM STATE VARIABLES AND SONIC SPEEDS IN CHEMICALLY REACTING AIR, FOR APPLICATIONS IN CFD.

J. M. Anderson
Department of Aerospace Engineering,
The University, Glasgow, G12 8QQ.
Report No. 9206
February 1992

Abstract.

This report presents a fast technique for calculating the equilibrium thermochemical state of air at high temperatures. The method has been developed for applications in computational fluid dynamics. A six species, three reaction air model is considered, with ionisation of the primary species neglected as a concession to reduced computing times.

Both curve fits and statistical expressions are considered for the calculation of the species thermodynamic properties in the range 200 K to 15 000 K. Curve fits are selected as the more efficient technique for evaluating these properties at high temperatures. The temperature range is subdivided into three regions and distinct models for the thermochemical behaviour of air are solved in each region to give the concentrations of the six species. The species properties and concentrations are then used to compute the specific properties of the mixture. The equilibrium and frozen speeds of sound are also calculated. A technique for inverting the state equations is then developed to allow the method to be applied to finite difference algorithms for air flow problems.

The scheme is validated against curve fit data and Mollier charts for the high temperature properties of equilibrium air.

Nomenclature.

a_{ij}	curve fit coefficients	
b_i	polynomial coefficients	
c_f	frozen speed of sound	m s^{-1}
c_e	equilibrium speed of sound	m s^{-1}
c_p	specific heat at const. pressure	J kg^{-1} K^{-1}
$\hat{c}_p$	molar heat at const. pressure	J mol^{-1} K^{-1}
$\hat{c}_v$	molar heat at const. volume	J mol^{-1} K^{-1}
e	specific internal energy	J kg^{-1}
$\hat{e}$	molar internal energy	J mol^{-1}
$\hat{e}_f^0$	energy of formation at absolute zero	J mol^{-1}
$\Delta\hat{e}_R^0$	heat of reaction at absolute zero	J mol^{-1}
E	specific total energy	J kg^{-1}
F	flux vector	
g	degeneracy	
$\hat{g}$	molar Gibbs free energy	J mol^{-1}
$\hat{g}^0$	molar Gibbs free energy at standard state	J mol^{-1}
h	specific enthalpy	J kg^{-1}
$\hat{h}$	molar enthalpy	J mol^{-1}
K	equilibrium constants in terms of specific concentrations	
K_p	equilibrium constants in terms of partial pressures	
$\hat{M}$	molar mass	kg mol^{-1}
p	pressure	N m^{-2}
p_0	standard state pressure	101 325 N m^{-2}
Q	partition function	
R	specific gas constant	J kg^{-1} K^{-1}
$\hat{R}$	universal gas constant	J mol^{-1} K^{-1}
s	specific entropy	J kg^{-1} K^{-1}
$\hat{s}$	molar entropy	J mol^{-1} K^{-1}
$\hat{s}^0$	molar entropy at standard state	J mol^{-1} K^{-1}
T	temperature	K
T_0	standard state temperature	273.15 K
u	fluid velocity	m s^{-1}
U	vector of conserved variables	
x	mole fraction	
γ	ratio of specific heats	
η	specific concentration	mol kg^{-1}
θ	charactersitic temperature	K
ι	ionisation parameter	J^2 kg^{-2} K^{-1}
ν	stoichiometric coefficients	
ρ	density	kg m^{-3}
σ	symmetry factor	

1) Introduction.

At subsonic and low supersonic flight speeds, the thermodynamic behaviour of air can be modelled sufficiently accurately using ideal gas theory. Behind this lies the assumption that air is composed of rigid rotating diatomic molecules. There is no facility within such a model to take account of important high temperature effects, such as electronic or vibrational excitation, or chemical decomposition. Below temperatures of about 620 K, equivalent to the temperature behind a normal shock wave at M = 2.5 under standard sea level conditions, these effects are indeed negligible. It will be shown that below this temperature, the equilibrium constants for the major chemical reactions in air are too small to be represented by a sixteen byte floating point number, and the concentrations of the associated substances can therefore be assumed to be zero.

The atmospheric entry trajectories of space vehicles can lead to Mach numbers in excess of 25, and so a real gas model of air becomes essential in this case. The form of the model chosen depends on several factors, the most important of which are the time taken to evaluate the necessary information and the amount of information provided. For the time dependent finite difference algorithms commonly used for the steady state solution of fluid dynamic problems, there is a need for fast algorithms in order to approach the steady state quickly, then for accurate algorithms which provide a smooth converged solution. Ref. 1 presents details of the application of curve fit techniques to computational schemes for solving the Euler equations. This report outlines a more physical approach to calculating the thermodynamic state of high temperature air. The scheme is suitable for applications in finite difference codes either in post processing to provide additional chemical data, or within the solution algorithm to provide smooth converged solutions with a maximum of physical input.

2) High Temperature Air.

Consideration is given to developing an algorithm which can compute the thermochemical state of air in equilibrium, suitable for applications in high speed aerodynamics. It is most likely that such flight conditions occur in reentry problems at high altitude. This suggests that conditions of low density and high temperature will prevail. These conditions tend to minimalize the effects of intermolecular forces, and allow each component of air to be treated as a thermally perfect gas. No corrections for the virial coefficients of the component gases are presented. That is to say, air itself is a thermally and calorically imperfect gas, so that its specific heats are functions of temperature and density, but the component species

are treated as being calorically imperfect only, so that their specific heats are functions of temperature.

Furthermore, low density air flows will tend to have longer relaxation times for chemical and vibrational processes, due to the larger intermolecular spacing and lower collision frequencies at a given temperature. This implies that very high speed, high altitude flows will have to be modelled with nonequilibrium thermochemistry. It is unlikely that ionisation phenomena, which are excited at low densities and high temperatures, will occur in regimes where the flow can validly be modelled in equilibrium. When this fact is combined with the need to have a fast set of routines for calculating the thermochemical state of the gas, it becomes advantageous to exclude ionisation phenomena from the model and restrict its application accordingly.

The model chosen to represent air involves the following six species: diatomic oxygen O_2, diatomic nitrogen N_2, monatomic oxygen O, nitrous oxide NO, monatomic nitrogen N and argon Ar. All ionised species and trace species such as carbon dioxide, water vapour and ozone are ignored. Table 1 gives the atomic weights of these species, together with their low temperature concentrations.

			Proportions at T = 273.15 K	
Species Number	Species	Molar Mass $\hat{M}$ (kg mol^{-1})	Mole Fraction x	Mass Fraction α
1	O_2	0.031999	0.2095	0.2314
2	N_2	0.028013	0.7809	0.7553
3	O	0.015999	0.0000	0.0000
4	NO	0.030006	0.0000	0.0000
5	N	0.014007	0.0000	0.0000
6	Ar	0.039948	0.0096	0.0133
Molar Mass of Air at 273.15 K = $\Sigma(x_i\hat{M}_i)$ = 0.028963 kg mol^{-1}				

Table 1) Low Temperature Composition of Air.

Argon is treated as an inert gas, and does not participate in any reactions. It does, however, make a contribution to the internal energy of the gas mixture which must be accounted for. The reactions which take place between the above species are:

$$O_2 + X \leftrightarrow 2O + X \qquad \Delta\hat{e}_R{}^0 = 493.566 \text{ kJ mol}^{-1} \qquad (2.1)$$

$$N_2 + O_2 + X \leftrightarrow 2NO + X \qquad \Delta\hat{e}_R{}^0 = 181.342 \text{ kJ mol}^{-1} \qquad (2.2)$$

$$N_2 + X \leftrightarrow 2N + X \qquad \Delta\hat{e}_R{}^0 = 941.636 \text{ kJ mol}^{-1} \qquad (2.3)$$

In these reactions, species X represents a catalytic body which is present only to act as an energy source for the reaction. For example, diatomic oxygen cannot spontaneously decompose into oxygen atoms - a catalyst must collide with the molecule and supply sufficient energy to break the atomic bond. This catalytic body may be any atom or molecule present in the mixture and, for an equilibrium calculation, is of little significance. It is, however, vitally important in nonequilibrium calculations, where different catalysts yield different reaction rates. The $\Delta\hat{e}_R{}^0$ above are the heats of reaction at absolute zero for the three reactions.

3) Thermodynamic Properties of the Component Species.

As already mentioned the six components of the air model are treated as thermally perfect, but calorically imperfect. It is necessary to calculate the thermodynamic properties of each species (internal energies, enthalpies, Gibbs free energies and specific heats). Two methods of calculating these properties have been investigated, each with its own relative merits.

The first method, and potentially the most accurate, is to evaluate these properties from statistical mechanical data [Ref. 2]. Energy contributions due to the different modes within an atom or molecule can be evaluated from their partition functions using the relations:

$$\hat{e} = \hat{R}\, T^2 \frac{\partial}{\partial T} \ln Q + \hat{e}_f{}^0 \qquad (3.1)$$

$$\hat{c}_v = \left(\frac{\partial \hat{e}}{\partial T}\right)_\rho \qquad (3.2)$$

where $\hat{e}$ is the molar internal energy, $\hat{c}_v$ is the molar heat at constant volume and Q is the statistically evaluated partition function. The partition function for each species can be broken down into components representing the individual energy modes within the atom or molecule, which yield expressions of the form [Ref. 3]:

$$Q_{translational} = V\left(\frac{2\pi mkT}{h^2}\right)^{3/2} \qquad (3.3)$$

$$Q_{electronic} = \sum_{i\geq 0} g_i\, e^{-\theta_i/T} \qquad (3.4)$$

$$Q_{rotational} = \frac{1}{\sigma}\left(\frac{T}{\theta_r}\right) \qquad (3.5)$$

$$Q_{vibrational} = \frac{1}{1 - e^{-\theta_v/T}} \qquad (3.6)$$

In equation (3.5), σ is a symmetry factor and is 1 for heteronuclear molecules and 2 for homonuclear molecules [Ref 2]. Rotational and vibrational contributions can apply only to the diatomic species. These partition functions give the molar heats and internal energies for diatomic species in the from:

$$\hat{c}_v = \hat{R}\left[\frac{3}{2} + \frac{1}{(\sum_i g_i e^{-\theta_i/T})^2} \sum_{i>j} \sum_j \left(g_i \frac{\theta_i}{T} - g_j \frac{\theta_j}{T} \right)^2 e^{-(\theta_i+\theta_j)/T} + 1 + \left(\frac{\theta_v/T}{e^{\theta_v/2T} - e^{-\theta_v/2T}} \right)^2 \right] \qquad (3.7)$$

$$\hat{e} = \hat{R}T\left[\frac{3}{2} + \frac{1}{\sum_i g_i e^{-\theta_i/T}} \sum_i g_i \frac{\theta_i}{T} e^{-\theta_i/T} + 1 + \frac{\theta_v/T}{e^{\theta_v/T} - 1} \right] + \hat{e}_f^{\,0} \qquad (3.8)$$

It is noted that the above expressions are based on an harmonic oscillator model of the vibrational modes, and no account is taken of coupling effects between the rotation and vibration in diatomic molecules. Contributions due to electronic excitation are in an open ended form, and it is desirable only to consider those terms in the series which contribute significantly to $\hat{c}_v$ or $\hat{e}$. From a practical point of view, it is necessary to limit the number of terms in this series to avoid lengthy computing times for $\hat{c}_v$. Table 2 presents the data used to calculate $\hat{c}_v$ and $\hat{e}$ for the six species in table 1 [Ref. 4].

Species	θ_1 (K)	θ_2 (K)	g_0	g_1	g_2	σ	θ_r (K)	θ_v (K)	$\hat{e}_f^{\,0}$ (kJ mol^{-1})
O_2	11 390		3	2		2	2.1	2 270	0.0
N_2			1			2	2.9	3 390	0.0
NO	174		2	2		1	2.5	2 740	90.671
O	228	326	5	3	1				246.783
N			4						470.818
Ar			1						0.0

Table 2) Statistical Constants for the Main Chemical Components of Air.

To give the desired computational speed, a maximum of three terms (including the constant term g_0) are retained in the electronic partition functions. High temperature electronic effects, anharmonic effects and coupling effects are therefore neglected. This leads to errors

at temperatures above 6000 K, particularly notable in the $\hat{c}_v$ variations. Figure 1 presents the distribution of $\hat{c}_v$ calculated from (3.7) for 200 K to 6000 K. Monatomic gases are observed to have $\hat{c}_v = {}^3/_2 (R,\hat{}) \approx 12.5$ J mol^{-1} K^{-1} at 200 K and diatomic gases have $\hat{c}_v = {}^5/_2 \hat{R} \approx 20.8$ J mol^{-1} K^{-1}. At this temperature rotation is fully excited in diatomic molecules, and there is some small electronic contribution, notably in species containing oxygen. Vibrational modes excite at temperatures between 400 K and 2000 K, giving a smooth rise in $\hat{c}_v$ up to about 29.1 J mol^{-1} K^{-1} for diatomic species. Departures from this value are due to electronic effects, most notable in O_2. Corresponding data for $\hat{e}$ are presented in figure 3.

The second, and preferred, technique for calculating the species properties relies on fitting polynomial curves to statistically calculated data. This has the advantage of improving the accuracy of the calculations, at the expense of some physical input. It was pointed out earlier that the statistical mechanics approach described above is potentially more accurate, but this has to be traded against increased computing times. Applying a curve fit to detailed calculations of the species properties allows a fast close approximation to them, which can extend the range of the model at no additional computational expense. This is the approach adopted in Ref. 5, and the curve fits presented in that reference are used here. Additional curve fits are presented in Ref. 6, but these are formulated in terms of the total number density, and as such are not suited to an equilibrium calculation, unless it is based on an iterative quasi-nonequilibrium method.

A fifth order polynomial in T is fitted to data for $\hat{c}_p$ and the required properties are calculated as follows. It is first noted that $\hat{c}_p$ is a function of temperature only so that:

$$\hat{c}_p(T) = \left(\frac{\partial \hat{h}}{\partial T}\right)_p = \hat{R} \sum_{j=1}^{5} a_j T^{j-1} \tag{3.9}$$

The differential relationships:

$$d\hat{h} = \hat{c}_p(T)\, dT \tag{3.10}$$

$$d\hat{s} = \hat{c}_p(T) \frac{dT}{T} - \hat{R} \frac{dp}{p} \tag{3.11}$$

lead to:

$$\hat{h} = \int_{T0}^{T} \hat{c}_p(T)\, dT + \hat{h}_f^{T0}$$

$$= \hat{R}\left[\sum_{j=1}^{5} \frac{a_j}{j} T^j + a_6 \right] \tag{3.12}$$

and:

$$\hat{s}^0 = \int_{T_0}^{T} \frac{\hat{c}_{p(T)}}{T} dT + \hat{s}^{T_0}$$

$$= \hat{R}\left[a_1 \ln T + \sum_{j=2}^{5} \frac{a_j}{j-1} T^{j-1} + a_7 \right] \qquad (3.13)$$

Data are available for curve fits in this form for temperatures in the range 200 K to 15 000 K [Ref. 5]. At temperatures at or below about 300 K, the statistical mechanics approach with the data presented in table 2 will yield more accurate results, down to temperatures approaching θ_r (generally of the order of 3 K for the gases considered). However, such low temperatures are very unlikely to be encountered in trans-atmospheric flight, and will be associated with thermal imperfections in the species behaviour which invalidate the present method. The curve fit approach is therefore adopted as it is more efficient at high temperatures. Figure 2 is provided for comparison with the statistical data on $\hat{c}_v$ in the range 200 K to 6 000 K. Figure 4 presents the data for $\hat{e}$ throughout the full range of the curve fits and compares with the statistical calculation in figure 3.

The molar heats $\hat{c}_v$ are plotted throughout the range 200 to 15 000 K in figure 5 using the curve fit data, from which it is observed that the neglect of high temperature terms in the electronic partition functions has a pronounced effect on both monatomic and diatomic species characteristics. Diatomic species are further influenced by both coupling and anharmonic effects, therefore the simplified statistical expressions cannot be considered valid at temperatures above about 8 000 K.

4) Equilibrium Species Concentrations.

The method used for calculating the equilibrium species concentrations is a modified version of that presented in Ref. 5 and 7. The chemical equilibrium equations, corresponding to reactions (2.1) to (2.3) are combined with mass conservation equations to give a non-linear set of algebraic equations for the equilibrium concentrations.

The equilibrium equations associated with the three reactions under consideration are as follows [Ref. 8]:

$$K_{p1} = \frac{(p_3/p_0)^2}{(p_1/p_0)} \qquad (4.1)$$

$$K_{p2} = \frac{(p_4/p_0)^2}{(p_1/p_0)(p_2/p_0)} \tag{4.2}$$

$$K_{p3} = \frac{(p_5/p_0)^2}{(p_2/p_0)} \tag{4.3}$$

The p_i represent the partial pressures of each species i (see table 1) and the K_{p_j} are the equilibrium constants for reactions 1 to 3, evaluated at standard state pressure $p_0 = 101\ 325\ N\ m^{-2}$. It is more convenient to work in mole mass ratios η_i rather than partial pressures, so the relation:

$$p_i = \eta_i \rho \hat{R} T \tag{4.4}$$

is applied to give:

$$\frac{\eta_3^2}{\eta_1} = \frac{p_0}{\rho \hat{R} T} K_{p1} = K_1 \tag{4.5}$$

$$\frac{\eta_4^2}{\eta_1 \eta_2} = K_{p2} = K_2 \tag{4.6}$$

$$\frac{\eta_5^2}{\eta_2} = \frac{p_0}{\rho \hat{R} T} K_{p3} = K_3 \tag{4.7}$$

The K_{p_j} are related to the species properties through the Gibbs free energy in the standard state:

$$\Delta \hat{g}_j^0 = -\hat{R}\, T \ln K_{p_j} \tag{4.8}$$

If the reactions are written in the form:

$$\sum_{i=1}^{N} \nu_i' X_i \leftrightarrow \sum_{i=1}^{N} \nu_i'' X_i \tag{4.9}$$

then the free energy change $\Delta \hat{g}_i^0$ will be given by:

$$\Delta \hat{g}_i^0 = \sum_i \nu_i'' \hat{g}_i^0 - \sum_i \nu_i' \hat{g}_i^0 \tag{4.10}$$

The $\hat{g}_i^0$ represent the standard state free energy for species i and can be evaluated from the species properties already presented:

$$\hat{g}_i^0 = \hat{h}_i - T \hat{s}_i^0 \tag{4.11}$$

For any given temperature and density, equations (4.5) to (4.7) provide three equations for the five unknown mole mass ratios η_i. As already stated, argon is considered to be inert in this case and so η_6 has a fixed value corresponding to the low temperature concentration of the species. Two further equations are required before the problem is fully defined. These follow from the nuclear conservation equations, relating the number of oxygen and nitrogen nuclei under any condition to their low temperature concentrations:

$$2\eta_1 + \eta_3 + \eta_4 = \eta_O \tag{4.12}$$

$$2\eta_2 + \eta_4 + \eta_5 = \eta_N \tag{4.13}$$

$$\eta_6 = \eta_{Ar} \tag{4.14}$$

These six equations, (4.5) to (4.7) and (4.12) to (4.14), can be combined and solved to yield the mole mass ratios, or specific concentrations, of the species at any temperature and density.

5) Low Temperature Considerations.

In the solution of the six equilibrium equations, the ratio $K_2/(K_1K_3)$ occurs frequently, and care is therefore required at low temperatures, where the concentration of monatomic nitrogen and oxygen tend to zero. This results in a division by zero error when K_1 or K_3 is smaller than a machine representable number. This problem is circumvented by assuming that if the natural log of K_{p3} is less than -100, reaction 3 does not take place and similarly if the natural log of K_{p1} is less than -100 then reaction 1 does not occur. Figure 6 shows the temperature variation of the reaction constants between 200 K and 15 000 K. From this it can be deduced that below about 530 K neither reaction 1 nor reaction 3 can be simulated and below 1 000 K only reaction 3 cannot be simulated. There are therefore three cases to be considered.

1) Very low temperature: $\ln K_{p1} < -100$, $T < 530$ K.

In this case reactions 1 and 3 do not occur. Mole mass ratios for O and N are correspondingly set to zero, and the remaining mole mass ratios are calculated from the equilibrium balance of reaction 2.

assumption:

$$\eta_3 = 0 \tag{5.1}$$

$$\eta_5 = 0 \tag{5.2}$$

equilibrium:

$$\frac{\eta_4^2}{\eta_1\eta_2} = K_2 \tag{5.3}$$

nuclear conservation:

$$2\eta_1 + \eta_4 = \eta_O \quad (5.4)$$

$$2\eta_2 + \eta_4 = \eta_N \quad (5.5)$$

$$\eta_6 = \eta_{Ar} \quad (5.6)$$

2) Low temperature: $\ln K_{p3} < -100$, $T < 1\,000\ K$.

Reaction 1 now leads to some oxygen dissociation, and the assumption of negligable monatomic oxygen is no longer considered valid. Nitrogen dissociation has not yet begun.

assumption:

$$\eta_5 = 0 \quad (5.7)$$

equilibrium:

$$\frac{\eta_3^2}{\eta_1} = K_1 \quad (5.8)$$

$$\frac{\eta_4^2}{\eta_1\eta_2} = K_2 \quad (5.9)$$

nuclear conservation:

$$2\eta_1 + \eta_3 + \eta_4 = \eta_O \quad (5.10)$$

$$2\eta_2 + \eta_4 = \eta_N \quad (5.11)$$

$$\eta_6 = \eta_{Ar} \quad (5.12)$$

3) High temperature: $T > 1\,000\ K$

All three reactions are important and so the full solution for the six unknown mole mass ratios is required.

equilibrium:

$$\frac{\eta_3^2}{\eta_1} = K_1 \quad (5.13)$$

$$\frac{\eta_4^2}{\eta_1\eta_2} = K_2 \quad (5.14)$$

$$\frac{\eta_5^2}{\eta_2} = K_3 \quad (5.15)$$

$$2\eta_1 + \eta_3 + \eta_4 = \eta_O \quad (5.16)$$

$$2\eta_2 + \eta_4 + \eta_5 = \eta_N \quad (5.17)$$

$$\eta_6 = \eta_{Ar} \quad (5.18)$$

6) Solution of the Equilibrium Equations.

The solution of the equilibrium equations for the very low temperature case is a straight forward non-iterative process. Equations 5.3, 5.4 and 5.5 are combined to give:

$$\eta_4 = -\frac{(\eta_N + \eta_O) + \left[(\eta_N^2 + \eta_O^2) + (16/K_2 - 2)\eta_N\eta_O\right]^{1/2}}{2\,(4/K_2 - 1)} \qquad (6.1)$$

Mole mass ratios for the remaining unknown species follow from equations 5.4 and 5.5:

$$\eta_1 = 1/2(\eta_O - \eta_4) \qquad (6.2)$$

$$\eta_2 = 1/2(\eta_N - \eta_4) \qquad (6.3)$$

For the higher temperature models, it is not possible to solve the problem analytically, as above. Instead a fourth order polynomial in η_3 is solved using a Newton-Raphson iteration. This polynomial takes the form:

$$\sum_{j=0}^{4} b_j \eta_3^j = 0 \qquad (6.4)$$

where:

$$b_0 = 2K_1\eta_O^2 \qquad (6.5)$$

$$b_1 = (K_eK_3 - 4)K_1\eta_O \qquad (6.6)$$

$$b_2 = 2K_1 - K_eK_3K_1 - 8\eta_O - K_2(\eta_N - \eta_O) \qquad (6.7)$$

$$b_3 = 8 - K_2 - 2K_eK_3 \qquad (6.8)$$

$$b_4 = (8 - 2K_2)/K_1 \qquad (6.9)$$

and:

$$K_1K_3K_e^2 = K_2 \qquad (6.10)$$

The above coefficients relate to the high temperature model of air. In the low temperature case, the same polynomial is solved, but the coefficients are modified because the product K_3K_e must be set to zero.

An initial guessed value of η_3 is calculated by assuming η_5 is zero and that η_2 can be approximated by:

$$\eta_2 = \frac{\eta_N}{2} \qquad (6.11)$$

This leads to the equations:

$$2\eta_1 + \eta_3 + \eta_4' = \eta_O \qquad (6.12)$$

$$\eta_1 = \frac{\eta_3^2}{K_1} \qquad (6.13)$$

$$\frac{\eta_4'}{\eta_3} = \left(\frac{\eta_N K_2}{2K_1}\right)^{1/2} \qquad (6.14)$$

where η_4' is an approximate value of η_4. This initial guess is very good for the low temperature model where 6.11 is a good approximation. However, at higher temperatures, η_5 starts to become significant and the guess is consequently less accurate. However, it is observed that three iterations of a Newton-Raphson scheme is sufficient to provide a converged solution for η_3 in equation 6.4, even at high temperatures. From equations 6.12 to 6.14, the initial value of η_3 is given by:

$$\eta_3{}^1 = \left[\left\{ \frac{K_1}{4} + \left(\frac{\eta_N K_1 K_2}{32} \right)^{1/2} \right\}^2 + \frac{K_1 \eta_O}{2} \right]^{1/2} - \left\{ \frac{K_1}{4} + \left(\frac{\eta_N K_1 K_2}{32} \right)^{1/2} \right\} \quad (6.15)$$

Equation 6.4 is now solved in three iterations by the following Newton-Raphson algorithm:

$$f(\eta_3{}^n) = \sum_{j=0}^{4} b_j (\eta_3{}^n)^j \quad (6.16)$$

$$f'(\eta_3{}^n) = \sum_{j=1}^{4} j b_j (\eta_3{}^n)^{j-1} \quad (6.17)$$

$$\eta_3{}^{n+1} = \eta_3{}^n - \frac{f(\eta_3{}^n)}{f'(\eta_3{}^n)} \quad (6.18)$$

Having achieved a converged solution for η_3, the remaining unknown mole mass ratios follow algebraically. For the low temperature model, the unknowns are:

$$\eta_5 = 0 \quad (6.19)$$

$$\eta_4 = \eta_O - \eta_3 - \frac{2}{K_1} \eta_3{}^2 \quad (6.20)$$

$$\eta_2 = \frac{1}{2}(\eta_N - \eta_4) \quad (6.21)$$

$$\eta_1 = \frac{1}{2}(\eta_O - \eta_3 - \eta_4) \quad (6.22)$$

$$\eta_6 = \eta_{Ar} \quad (6.23)$$

For the high temperature model, they are:

$$\eta_5 = \frac{\eta_O - \eta_3 - \frac{2}{K_1} \eta_3{}^2}{K_e \eta_3} \quad (6.24)$$

$$\eta_4 = K_e \eta_3 \eta_5 \quad (6.25)$$

$$\eta_2 = \frac{1}{2}(\eta_N - \eta_4 - \eta_5) \quad (6.26)$$

$$\eta_1 = \frac{1}{2}(\eta_O - \eta_3 - \eta_4) \quad (6.27)$$

$$\eta_6 = \eta_{Ar} \quad (6.28)$$

Figures 7 to 9 illustrate the chemical composititon of air as calculated using the above method at densities of 1.225×10^{-4} kg m^{-3}, 1.225 kg m^{-3} and 122.5 kg m^{-3}. These are plots of mole fractions against temperature in the range 200 K to 15 000 K. The relationship between the mole fractions and mole mass ratios is:

$$x_i = \frac{\eta_i}{\sum_{j=1}^{6} \eta_j} \tag{6.29}$$

With the chemical properties of the gas mixture now known, it is possible to calculate the associated thermodynamic properties.

7) Thermodynamic Properties of the Mixture.

Having calculated the equilibrium chemical properties of the mixture for a given temperature and density, it is possible to compute the mixture thermodynamic properties. Of particular importance are the pressure and internal energy, but any thermodynamic variable can be calculated from the available information. The specific concentration (mole mass ratio) of the mixture is given by:

$$\eta = \sum_{i=1}^{6} \eta_i \tag{7.1}$$

Pressure can then be found from the thermal state equation in the form:

$$p = \hat{R}\, \eta\, \rho\, T \tag{7.2}$$

Specific enthalpy is given by:

$$h = \sum_{i=1}^{6} \hat{h}_i\, \eta_i \tag{7.3}$$

and specific internal energy follows from:

$$e = h - \hat{R}\, \eta\, T \tag{7.4}$$

The calculation of the mixture entropy is more complex. Returning to the differential form of the second law of thermodynamics, for a single species i:

$$T\, ds_i = dh_i - \frac{dp_i}{\rho} \tag{7.5}$$

or, since $s_i = \eta_i \hat{s}_i$, $p_i = \hat{R}\eta_i \rho T$ and $dh_i = \eta_i \hat{c}_{p_i} dT$:

$$d\hat{s}_i = \hat{c}_{pi} \frac{dT}{T} - \hat{R} \frac{dp_i}{p_i} \tag{7.6}$$

Integrating this expression then gives:

$$\hat{s}_i = \int_{T_0}^{T} \frac{\hat{c}_p}{T} dT - \hat{R} \int_{p_0}^{p_i} \frac{1}{p_i} dp_i + \hat{s}_i^{T_0} \tag{7.7}$$

The first and last terms on the right hand side of this equation are recognised from equation (3.13) to be the standard state entropy at $p_i = p_0$. Equation (7.7) therefore becomes:

$$\hat{s}_i = \hat{s}_i^0 - \hat{R} \ln \frac{p_i}{p_0} \tag{7.8}$$

The mixture specific entropy will be the summation of the species entropies multiplied by their respective concentrations:

$$s = \sum_i \eta_i \hat{s}_i$$

$$s = \sum_i \left(\eta_i \hat{s}_i^0 - \hat{R} \eta_i \ln \frac{p_i}{p} - \hat{R} \eta_i \ln \frac{p}{p_0} \right)$$

$$s = - \hat{R} \eta \ln \frac{p}{p_0} + \sum_i \eta_i \left(\hat{s}_i^0 - \hat{R} \ln \frac{p_i}{p} \right) \tag{7.9}$$

The partial pressures can be written in terms of mole mass ratios through an application of the thermal state equation (7.2):

$$\ln \frac{p_i}{p} = \ln \frac{\hat{R} \eta_i \rho T}{\hat{R} \eta \rho T} = \ln \eta_i - \ln \eta \tag{7.10}$$

Equation (7.9) can now be expressed in terms of total pressure and mole mass ratios:

$$s = - \hat{R} \eta \ln \frac{p}{\eta p_0} + \sum_i \eta_i \left(\hat{s}_i^0 - \hat{R} \ln \eta_i \right) \tag{7.11}$$

The Gibbs free energy can also be calculated for the mixture:

$$g = h - Ts \tag{7.12}$$

Figure 10 illustrates the application of these equations to compute an enthalpy-entropy diagram. Lines of constant temperature and constant density are plotted against calculated values of enthalpy and entropy. The resulting chart has been compared with Ref. 11 and gives good agreement, as shown by the results in table 3. It is noted, however, that the

flattening of the chart in figure 10 at high enthalpies and entropies is due to the mixture becoming fully dissociated and no further chemical changes taking place. This region of the chart is inaccurate, because of the lack of an ionisation model. It is, however, useful to have an approximate prediction of conditions in this region, even without ionisation modelled, in case the method should be used by a CFD code which allows accurate modelling within the general flow field, but where one or two points lie outside the valid enthalpy entropy range.

A useful indication of when ionisation is likely to become important is to evaluate the product of enthalpy and entropy, and compare this to the parameter:

$$\iota = h\,s > 9.2 \times 10^{-6}\ J^2\,kg^{-2}\,K^{-1} \qquad (7.13)$$

		Enthalpy / 10^6 (J kg^{-1})			Entropy / 10^3 (J kg^{-1} K^{-1})		
Density ($kg\ m^{-3}$)	Temp. (K)	Mollier Chart	Calculated Value	Difference x 10^3	Mollier Chart	Calculated Value	Difference x 10^3
12.88	1000	1.0470	1.0535	6.5	7.1185	7.1277	9.2
	2000	2.2673	2.2928	25.5	7.7526	7.7800	27.4
	3000	3.7001	3.7344	34.3	8.2137	8.2435	29.8
	6000	10.226	10.325	99.0	9.4530	9.4843	31.3
	8000	16.083	16.101	18.0	10.182	10.176	6.0
	12000	32.907	32.735	172.0	11.715	11.698	17.0
0.1288	1000	1.0470	1.0535	6.5	8.4299	8.4544	24.5
	2000	2.2751	2.2956	20.5	9.0783	9.1082	29.9
	3000	4.0543	4.0785	24.2	9.6605	9.6910	30.5
	6000	13.407	13.542	135.0	11.514	11.572	58.0
	8000	30.939	30.862	75.0	13.790	13.782	8.0
1.288×10^{-4}	1000	1.0470	1.0535	6.5	10.404	10.445	41.0
	2000	2.3617	2.3900	28.3	11.096	11.147	51.0
	3000	6.9514	7.0344	83.0	12.753	12.818	65.0

Table 3) Validation Data from Ref. 11†.

---

† The data presented in Ref. 11 are derrived for argon free air, and low temperature constants given by:

$T_0 = 273.16$ K, $\rho_0 = 1.288$ kg m^{-3}, $\hat{M} = 28.858\ 7$ g mol^{-1}.

The calculated values in table 3 are based on these conditions, and are therefore consistent with that reference.

8) Equilibrium and Frozen Speeds of Sound.

In an equilibrium flow calculation, it is important to be able to correctly evaluate the propagation speed of accoustic waves, particularly if a flux splitting technique is being employed [Ref. 9]. Also, the frozen speed of sound is important in nonequilibrium problems, and it is desirable to have a method for calculating this parameter at the equilibrium condition†.

The equilibrium and frozen speeds of sound are given by the expressions:

$$c_e^2 = \left(\frac{\partial p}{\partial \rho}\right)_{s,\eta=\eta^*} \tag{8.1}$$

$$c_f^2 = \left(\frac{\partial p}{\partial \rho}\right)_{s,\eta} \tag{8.2}$$

The constraints $\eta = \eta^*$ and η = constant must be imposed on the pressure derivative as well as the familiar constraint on entropy being constant because in a chemically active gas, any thermodynamic variable is a function of not only any two other state variables, but also the chemical state of the gas. Imposing these constraints therefore leads to unique values for the pressure derivative, one of which premits an infinitely fast adjustment of the chemical state of the gas (c_e) and the other of which premits no chemical changes (c_f). The two propagation speeds therefore lie at extreme opposite ends of the range of speeds at which a sound wave may propagate in a nonequilibrium gas.

Considering an equilibrium chemically reacting gas, the first and second laws of thermodynamics lead to the relation [Ref. 10].

$$T\,ds = de - \frac{p}{\rho^2}\,d\rho \tag{8.3}$$

---

† In a purely equilibrium calculation, the frozen speed of sound is meaningless because the gas is, by definition, constrained to remain always in equilibrium. If account is taken of nonequilibrium effects, then high frequency components of an accoustic wave will propagate into the equilibrium free stream at the frozen speed of sound, and this becomes an important parameter. The ratio of the frozen to equilibrium speed of sound gives an indication of how much an accoustic wave will distort due to nonequilibrium effects. It is therefore a useful pointer as to whether an equilibrium or fully nonequilibrium model should be employed, and as such the expressions developed to represent both frozen and equilibrium accoustic speeds are presented here.

this is equally valid for perfect, frozen or equilibrium gas models. In terms of enthalpy, this expression is:

$$T\,ds = dh - \frac{1}{\rho}\,dp \tag{8.4}$$

The enthalpy of the reacting gas mixture has already been expressed as a function of temperature and the chemical state of the gas, in terms of the mole mass ratios. That is:

$$h = h\,(T, \eta_i) \tag{8.5}$$

$$dh = (h)_T\,dT + \sum_{i=1}^{6} (h)_{\eta_i}\,d\eta_i \tag{8.6}$$

where:

$$(h)_T = \left(\frac{\partial h}{\partial T}\right)_{\eta_i} \tag{8.7}$$

$$(h)_{\eta_i} = \left(\frac{\partial h}{\partial \eta_i}\right)_{T,\eta_{j\neq i}} \tag{8.8}$$

Furthermore, the species mole mass ratios in equilibrium are functions only of temperature and density:

$$\eta_i = \eta_i\,(\rho, T) \tag{8.9}$$

$$d\eta_i = (\eta_i)_\rho\,d\rho + (\eta_i)_T\,dT \tag{8.10}$$

where:

$$(\eta_i)_\rho = \left(\frac{\partial \eta_i}{\partial \rho}\right)_T \tag{8.11}$$

$$(\eta_i)_T = \left(\frac{\partial \eta_i}{\partial T}\right)_\rho \tag{8.12}$$

The thermal state equation for a chemically reacting gas can be written:

$$p = \hat{R} \sum_{i=1}^{6} \eta_i\,\rho\,T \tag{8.13}$$

which in differential form becomes:

$$dp = \hat{R}\left(\sum_{i=1}^{6} \eta_i\,\rho\,dT + \sum_{i=1}^{6} \eta_i\,T\,d\rho + \rho\,T \sum_{i=1}^{6} d\eta_i \right) \tag{8.14}$$

Putting equation (8.10) into (8.14) yields:

$$dT = \frac{1}{\left[\eta + T \sum_i (\eta_i)_T\right]} \frac{dp}{\hat{R}\rho} - \frac{\left[\eta + \rho \sum_i (\eta_i)_\rho\right]}{\left[\eta + T \sum_i (\eta_i)_T\right]} \frac{T\, d\rho}{\rho} \qquad (8.15)$$

From (8.6) and (8.10):

$$dh = \left[(h)_T + \sum_i (h)_{\eta_i} (\eta_i)_T\right] dT + \left[\sum_i (h)_{\eta_i} (\eta_i)_\rho\right] d\rho \qquad (8.16)$$

Putting (8.15) into (8.16), then applying the resulting expression for dh to the Tds equation in the form of (8.4) gives an expression for ds as a function of dp and dρ:

$$\begin{aligned}\left[\eta + T \sum_i (\eta_i)_T\right] T\, ds = {} & \left\{\frac{1}{\hat{R}\rho}\left[(h)_T + \sum_i (h)_{\eta_i}(\eta_i)_T\right] - \frac{1}{\rho}\left[\eta + T \sum_i (\eta_i)_T\right]\right\} dp - \\ & \left\{\frac{T}{\rho}\left[(h)_T + \sum_i (h)_{\eta_i}(\eta_i)_T\right]\left[\eta + \rho \sum_i (\eta_i)_\rho\right] - \right. \\ & \left. \left[\sum_i (h)_{\eta_i}(\eta_i)_\rho\right]\left[\eta + T \sum_i (\eta_i)_T\right]\right\} d\rho \end{aligned} \qquad (8.17)$$

The equilibrium speed of sound is given by setting ds in (8.17) to zero:

$$\begin{aligned}\left(\frac{\partial p}{\partial \rho}\right)_{s,\eta_i=\eta_i^*} = {} & \frac{\hat{R}T\left[(h)_T + \sum_i (h)_{\eta_i}(\eta_i)_T\right]\left[\eta + \rho \sum_i (\eta_i)_\rho\right]}{\left[(h)_T + \sum_i (h)_{\eta_i}(\eta_i)_T\right] - \hat{R}\left[\eta + T \sum_i (\eta_i)_T\right]} - \\ & \frac{\hat{R}\rho\left[\sum_i (h)_{\eta_i}(\eta_i)_\rho\right]\left[\eta + T \sum_i (\eta_i)_T\right]}{\left[(h)_T + \sum_i (h)_{\eta_i}(\eta_i)_T\right] - \hat{R}\left[\eta + T \sum_i (\eta_i)_T\right]} \end{aligned} \qquad (8.18)$$

Equation (8.18) gives c^2 for an equilibrium gas. If the gas is frozen in any chemical state, the derivatives $(\eta_i)_T$ and $(\eta_i)_\rho$ will be zero, since no change in the chemistry of the gas can occur. Equation (8.18) then reduces to:

$$\left(\frac{\partial p}{\partial \rho}\right)_{s,\eta_i} = \frac{\hat{R}\eta T (h)_T}{(h)_T - \hat{R}\,\eta} \qquad (8.19)$$

which is c^2 in a frozen gas.

Furthermore, it is interesting to note that the product $\hat{R}\eta$ is the specific gas constant R and, from 8.7, $(h)_T$ is the specific heat c_p for a chemically inert gas. If 8.18 is simplified to the perfect gas case, the result is therefore:

$$\left(\frac{\partial p}{\partial \rho}\right)_{s,\eta_i} = \frac{c_p}{c_p - R} RT = \gamma RT \tag{8.20}$$

This is the familiar result for a nonreacting perfect gas.

Once the chemical composition of the gas has been calculated, it is necessary to calculate the thermodynamic derivatives appearing in equation (8.18). The mixture enthalpy is given by equation (7.3). With the species molar enthalpies from equation (3.12), this can be differentiated directly to give $(h)_T$:

$$(h)_T = \hat{R} \sum_{i=1}^{6} \eta_i \left(\sum_{j=1}^{5} a_{ij} T^{j-1} \right) \tag{8.21}$$

Similarly $(h)_{\eta_i}$ is given by:

$$(h)_{\eta_i} = \hat{R} \left(\sum_{j=1}^{5} \frac{a_{ij}}{j} T^{j-1} + a_{i6} \right) \tag{8.22}$$

Calculation of the derivatives $(\eta_i)_T$ and $(\eta_i)_\rho$ is less straight forward. In the very low temperature case, where the η_i are explicit functions of the equilibrium coefficient K_2 the derivatives are given by the differential forms of equations (5.1) to (5.5), which lead to:

$$\delta\eta_4 = \frac{2\eta_1\eta_2}{4\eta_4 + K_2(\eta_1 + \eta_2)} \delta K_2 \tag{8.23}$$

$$\delta\eta_1 = -\frac{1}{2}\delta\eta_4 \tag{8.24}$$

$$\delta\eta_2 = -\frac{1}{2}\delta\eta_4 \tag{8.25}$$

$$\delta\eta_3 = 0 \tag{8.26}$$

$$\delta\eta_5 = 0 \tag{8.27}$$

where δ represents either $\partial/\partial\rho$ or $\partial/\partial T$.

The equations representing the low temperature model, (5.7) to (5.11), can be written in differential form as:

$$2\eta_3\delta\eta_3 = K_1\delta\eta_1 + \eta_1\delta K_1 \tag{8.28}$$

$$2\eta_4\delta\eta_4 = K_2\eta_1\delta\eta_2 + K_2\eta_2\delta\eta_1 + \eta_1\eta_2\delta K_2 \tag{8.29}$$

$$2\delta\eta_1 + \delta\eta_3 + \delta\eta_4 = 0 \tag{8.30}$$

$$2\delta\eta_2 + \delta\eta_4 = 0 \tag{8.31}$$

This is a set of linear algebraic equations in the unknown chemical derivatives $\delta\eta_i$, which can be solved analytically to give:

$$\delta\eta_4 = \frac{\eta_1\eta_2\delta K_2 - \frac{\eta_1\eta_2}{2\eta_3}(K_1\delta K_2 - K_2\delta K_1)}{4\eta_4 + K_2(\eta_1 + \eta_2) + K_2\frac{\eta_2}{\eta_3} + \frac{1}{4}K_1K_2\frac{\eta_1}{\eta_3}} \tag{8.32}$$

$$\delta\eta_3 = \frac{2\eta_1\delta K_1 - K_1\delta\eta_4}{4\eta_3 + K_1} \tag{8.33}$$

$$\delta\eta_2 = -\frac{1}{2}\delta\eta_4 \tag{8.34}$$

$$\delta\eta_1 = -\frac{1}{2}(\delta\eta_3 + \delta\eta_4) \tag{8.35}$$

$$\delta\eta_5 = 0 \tag{8.36}$$

Unlike the low temperature models, in the high temperature case chemical derivatives must be found from the fourth order polynomial (6.4). Implicit differentiation of this equation leads to expressions for $(\eta_3)_T$ and $(\eta_3)_\rho$:

$$\delta\eta_3 = -\frac{\sum_{j=0}^{4}\delta b_j\eta_3^{\,j}}{\sum_{j=1}^{4} j b_j\eta_3^{\,j-1}} \tag{8.37}$$

The b_j are the coefficients in equation (6.4) and δb_j represent the temperature or density derivatives of these coefficients. The derivatives of these coefficients are found by differentiating equations (6.5) to (6.9).

$$\delta b_0 = 2\eta_O{}^2\delta K_1 \tag{8.38}$$

$$\delta b_1 = (K_eK_3 - 4)\eta_O\delta K_1 + K_1K_e\eta_O\delta K_3 + K_1K_3\eta_O\delta K_e \tag{8.39}$$

$$\delta b_2 = 2\delta K_1 - (\eta_N - \eta_O)\delta K_2 - K_3K_e\delta K_1 - K_1K_e\delta K_3 - K_1K_3\delta K_e \tag{8.40}$$

$$\delta b_3 = -\delta K_2 - 2K_3\delta K_e - 2K_e\delta K_3 \tag{8.41}$$

$$\delta b_4 = (-b_4\delta K_1 - 2\delta K_2)/K_1 \tag{8.42}$$

Having found $\delta\eta_3$ from the above expressions, the remaining chemical derivatives follow from equations (6.24) to (6.27) in differential form:

$$\delta\eta_5 = \frac{2\eta_3}{K_1^2 K_e}\delta K_1 - \left(\frac{\eta_5}{\eta_3} + \frac{4}{K_1 K_e} + \frac{1}{K_e \eta_3}\right)\delta\eta_3 - \frac{\eta_5}{K_e}\delta K_e \qquad (8.43)$$

$$\delta\eta_4 = \eta_3\eta_5\delta K_e + K_e\eta_5\delta\eta_3 + K_e\eta_3\delta\eta_5 \qquad (8.44)$$

$$\delta\eta_2 = -\frac{1}{2}(\delta\eta_4 + \delta\eta_5) \qquad (8.45)$$

$$\delta\eta_1 = -\frac{1}{2}(\delta\eta_3 + \delta\eta_4) \qquad (8.46)$$

In order to evaluate the above expressions for the chemical derivatives η_i, a knowledge of the derivatives of the equilibrium constants K_j is required. These are found from equations (4.8) and (6.10). From (6.10):

$$\delta K_e = \frac{K_e}{2K_2}\left[\,\delta K_2 - K_3 K_e^2\,\delta K_1 - K_1 K_e^2\,\delta K_3\,\right] \qquad (8.47)$$

From (4.5) to (4.8):

$$K_1 = \exp\left[\frac{\hat{g}_1^0}{\hat{R}T} - 2\frac{\hat{g}_3^0}{\hat{R}T} + \ln\frac{p_0}{\rho\hat{R}T}\right] \qquad (8.48)$$

$$K_2 = \exp\left[\frac{\hat{g}_1^0}{\hat{R}T} + \frac{\hat{g}_2^0}{\hat{R}T} - 2\frac{\hat{g}_4^0}{\hat{R}T}\right] \qquad (8.49)$$

$$K_3 = \exp\left[\frac{\hat{g}_2^0}{\hat{R}T} - 2\frac{\hat{g}_5^0}{\hat{R}T} + \ln\frac{p_0}{\rho\hat{R}T}\right] \qquad (8.50)$$

Differentiating these equations will lead to expressions involving the derivatives of the Gibbs free energies, defined according to equation (4.11). As the standard state free energies are a function only of temperature, their density derivatives are all zero. The temperature derivatives can be found most easily by replacing the enthalpy and entropy in (4.11) by definitions (3.12) and (3.13), giving:

$$\hat{g}^0 = \int_{T_0}^{T}\hat{c}_p\,dT + \hat{h}_f^{T_0} - T\int_{T_0}^{T}\frac{\hat{c}_p}{T}\,dT - T\,\hat{s}^{T_0} \qquad (8.51)$$

$$\frac{\partial}{\partial T}\left(\frac{\hat{g}^0}{\hat{R}T}\right) = \frac{\hat{c}_p}{\hat{R}T} - \frac{1}{\hat{R}T^2}\int_{T_0}^{T}\hat{c}_p\,dT - \frac{\hat{h}_f^{T_0}}{\hat{R}T^2} - \frac{\hat{c}_p}{\hat{R}T} \qquad (8.52)$$

$$\frac{\partial}{\partial T}\left(\frac{\hat{g}^{\theta}}{\hat{R}\,T}\right) = -\frac{\hat{h}}{\hat{R}\,T^2} \tag{8.53}$$

Utilising equation (8.53) for the five active species, and differentiating (8.48) to (8.50) with respect to temperature or density leads to:

$$\frac{\partial K_1}{\partial T} = \frac{K_1}{T}\left[\, 2\,\frac{\hat{h}_3}{\hat{R}T} - \frac{\hat{h}_1}{\hat{R}T} - 1 \,\right] \tag{8.54}$$

$$\frac{\partial K_2}{\partial T} = \frac{K_2}{T}\left[\, 2\,\frac{\hat{h}_4}{\hat{R}T} - \frac{\hat{h}_2}{\hat{R}T} - \frac{\hat{h}_1}{\hat{R}T} \,\right] \tag{8.55}$$

$$\frac{\partial K_3}{\partial T} = \frac{K_3}{T}\left[\, 2\,\frac{\hat{h}_5}{\hat{R}T} - \frac{\hat{h}_2}{\hat{R}T} - 1 \,\right] \tag{8.56}$$

$$\frac{\partial K_1}{\partial \rho} = -\frac{K_1}{\rho} \tag{8.57}$$

$$\frac{\partial K_2}{\partial \rho} = 0 \tag{8.58}$$

$$\frac{\partial K_3}{\partial \rho} = -\frac{K_3}{\rho} \tag{8.59}$$

All the chemical and thermodynamic derivatives appearing in equation (8.18) can now be calculated for each of the three air models, and it is therefore possible to compute the equilibrium speed of sound.

Equilibrium and frozen speed of sound variations with temperature are illustrated in figures 11 to 13, for three different densities. These show solutions of equations (8.18) and (8.19). For comparison, the perfect gas, $\gamma = 1.4$, solution is also shown. It is noted that the low density case (figure 11) exhibits perfect gas like behaviour at high temperatures. This is because the diatomic species become fully dissociated at these temperatures and no further chemical changes take place. This behaviour would be significantly modified if the presence of ionisation were modelled.

It is also interesting to note that the fully dissociated gas behaves like a perfect gas with $R = 571.4$ J kg^{-1} K^{-1} and $\gamma = 1.40$. This specific gas constant corresponds to that expected from the low temperature data in table 1. However, the value of γ for a fully monatomic gas would be expected to be 5/3 or 1.67. The departure from this value is explained by the high temperature behaviour of monatomic nitrogen, illustrated in figure 5. It is seen that the molar heat of nitrogen increases by about 8.5 J mol^{-1} K^{-1} due to electronic contributions to

the partition function. As this species composes over 78% of the gas, this causes the ratio of specific heats to fall significantly.

The ratio of sonic speeds, c_f/c_e, is plotted in figure 14. These curves show where the derivative terms in equation (8.18) are large, corresponding to the two peaks. These are the points of maximum dissociation rate (with respect to temperature) firstly for oxygen and then for nitrogen. It is possible that flight conditions giving sonic speed ratios at or near these points in large sections of the flow field will require to be modelled out of equilibrium.

9) Inversion of the State Equations.

The method of calculating the equilibrium thermochemical state of the gas mixture so far presented has been formulated on the basis that the independent variables are the fluid density and temperature. Mass density was chosen primarily for the following reasons. In a finite difference code, where the fluid flow equations are solved using a time dependent technique, the solution vector is given by:

$$\mathbf{U} = \begin{bmatrix} \rho \\ \rho u \\ \rho E \end{bmatrix} \tag{9.1}$$

where

$$E = e + \frac{u^2}{2}$$

The third element of (9.1) represents the total energy density, and is sometimes replaced by the total enthalpy density, depending on how the energy conservation equation has been formulated. On each iteration of the solution algorithm, this vector is updated numerically. It is then necessary to update the flux vector in preparation for the next iteration. The flux vector, for a one-dimensional case corresponding to (9.1), will be:

$$\mathbf{F} = \begin{bmatrix} \rho u \\ \rho u^2 + p \\ \rho u(E + p/\rho) \end{bmatrix} \tag{9.2}$$

From this it is clear that it is necessary to relate pressure, appearing in the flux vector, to internal energy and mass density in the solution vector. Thus density is a good choice as the first primary variable.

It would be advantageous to choose internal energy as the second thermodynamic variable. However this is not possible, because internal energy must be formulated in terms of temperature through equation (3.8). Temperature is a fundamental statistical variable. This

implies that there is no alternative to the use of temperature as the second thermodynamic variable used to specify the state of the system.

As a consequence of using mass density and temperature to specify the state of the system, a problem arises with relating the known mixture internal energy to the unknown temperature. This puts a limitation on the application of this model within a time dependent CFD code, because the only way of inverting the state equations is through an iterative numerical scheme [Ref. 1]. This inversion process must be repeated at every grid point, and therefore leads to a large amount of computing time spent on calculating a number of variables, many of which are not explicitly required in the solution algorithm.

Three inversion schemes were considered. These were a linear point iterative scheme, a superlinear Regula falsi method and a quadratic Newton-Raphson scheme [Ref 12.]. The first scheme was restricted by its slow convergence rate, and the second two methods were limited by their need for an accurate initial guess of temperature corresponding to the known internal energy. The choice between the Regula falsi and Newton-Raphson techniques was based on the fact that, for the Newton-Raphson technique, the chemical state of the gas needed to be calculated at only one point during the iteration. The Regula falsi technique required the chemistry to be analysed at an additional point on the temperature scale in order to calculate derivative information, and also required a more accurate initial guess. This offset the reduced amount of computation required because none of the thermochemical derivatives needed to be calculated. In addition, the Regula falsi method, being only superlinear, did not exhibit as fast a convergence rate as the quadratic Newton-Raphson scheme. The final choice of a Newton-Raphson scheme was therefore made.

The scheme is summarised as follows:

$$T^0 = T_{estimate}\,(\rho, e) \tag{9.3}$$

$$e^n = e^n\,(\rho, T^n) \tag{9.4}$$

$$\left(\frac{\partial e^n}{\partial T}\right)_\rho = \left(\frac{\partial}{\partial T}\, e^n(\rho, T^n)\right)_\rho \tag{9.5}$$

$$T^{n+1} = T^n - \frac{e^n - e}{(\partial e^n/\partial T)_\rho} \tag{9.6}$$

Details of the calculation of e as a function of ρ and T have already been presented in section seven. The energy derivative follows from the chemical state of the gas in a manner similar to that presented in section eight for the derivatives appearing in the accoustic equations.

Internal energy is a function of temperature and the chemical state of the gas, in an analogous fashion to equation (8.5):

$$e = e\,(T, \eta_i) \tag{9.7}$$

Then:

$$\left(\frac{\partial e}{\partial T}\right)_{\eta_i=\eta_i^*} = (e)_T + \sum_i (e)_{\eta_i}(\eta_i)_T \tag{9.8}$$

where

$$(e)_T = \left(\frac{\partial e}{\partial T}\right)_{\eta_i} \tag{9.9}$$

$$(e)_{\eta_i} = \left(\frac{\partial e}{\partial \eta_i}\right)_{T,\eta_{j\neq i}} \tag{9.10}$$

$$(\eta_i)_T = \left(\frac{\partial \eta_i}{\partial T}\right) \tag{9.11}$$

It is noted that the above derivatives are evaluated with mass density constant, so the chemical state of the system is a function of temperature only. Enthalpy and internal energy are related through:

$$e = h - \hat{R}\,\eta\,T \tag{9.12}$$

$$(e)_T = (h)_T - \hat{R}\,\eta \tag{9.13}$$

$$(e)_{\eta_i} = (h)_{\eta_i} - \hat{R}\,T\,(\eta)_{\eta_i} \tag{9.14}$$

In the above expressions $(h)_T$ and $(h)_{\eta_i}$ can be found from equations (8.21) and (8.22). The derivative $(\eta)_{\eta_i}$ is found from equation (7.1):

$$(\eta)_{\eta_i} = \sum_j^6 \left(\frac{\partial \eta_j}{\partial \eta_i}\right) = 1 \tag{9.15}$$

Equation (9.14) now reduces to:

$$(e)_{\eta_i} = (h)_{\eta_i} - \hat{R}\,T \tag{9.16}$$

Calculation of the chemical derivatives $(\eta_i)_T$ in equation (9.8) has already been discussed in section eight.

In order to initiate the iterative inversion of the scheme using this method, an accurate initial estimate of T is required. The most efficient way of doing this is to utilise an approximate curve fit. The current method uses the curve fits of Ref. 13. However, it is more efficient to use the less accurate curve fits of Ref. 14, as these involve less operations to evaluate and the loss in accuracy is not sufficient to cause the scheme to fail.

Figures 15 and 16 illustrate the results of calculating the equilibrium speed of sound and pressure from given specific internal energy and mass density. Temperature appears in this calculation only as an intermediate variable. A maximum of three iterations are required in the inversion process at low temperatures to achieve a converged solution to within 0.01 K. However, because the curve fits include the effects of ionisation, up to five iterations are required at higher temperatures. This less accurate† initial guess leads to the larger number of iterations. As can be seen from figures 15 and 16, the technique provides excellent smoothness and continuity throughout the valid range of densities and internal energies.

10) Validation.

The scheme presented here has been validated against the curve fits presented in Ref. 13, and the Mollier charts of Ref 11. For temperatures in the range 200 K to 15 000 K and densities from 1.225×10^{-6} kg m^{-3} to 1.225×10^{2} kg m^{-3} the equilibrium speed of sound, pressure and specific internal energy were calculated using the method presented here. The specified density and calculated internal energy were then applied to the curve fits of Ref. 13 to compute comparative values of pressure and equilibrium sonic speed. The data were then nondimensionalised consistently, and plotted in figures 17 and 18. In these figures, continuous lines represent the results of the current scheme, and crosses correspond to curve fit data.

From figure 17 it is clear that there is excellent agreement between the calculated and curve fit pressure data. There is some departure of the two methods at low densities and high energies, because of the presence of ionisation data in the curve fits.

A significant advantage of this scheme is evident from figure 18. The calculated sonic speed data are smooth and continuous throughout the applied temperature range. The curve fit

---

† This does not mean that the initial guess at high temperatures is physically inaccurate. Indeed, because of the inclusion of ionisation data, it is closer to the physically correct temperature than the the results of the method presented here. However, as an initial guess in the iterative inversion of the state equations for a model not including ionisation, it is far from the converged solution and is therefore termed "inaccurate".

data, because it relies on differentiating sets of discontinuous curves, cannot match this smoothness, and significant errors are apparent at junctions between curves - most noticeable at lower densities. Again the lack of an ionisation model in the present scheme accounts for the low density, high energy departures noted in figure 18, but otherwise agreement is very good.

11) Conclusions.

A fast method for calculating the thermochemical state of equilibrium air, including sonic speeds, has been presented. The method is well suited to post processing applications for fluid flow problems, where data on the chemical composition of the air are required. It is also suitable for inclusion in a time dependent iterative scheme, although it is not recommended unless some method, such as a curve fit technique, has been used to compute a good starting solution. This is because the amount of data required to calculate the thermodynamic state of the air is in excess of what is required by the flow solution algorithm. The number of calculations required to evaluate the thermodynamic state of the gas is therefore large in comparison to a curve fit technique.

The method presented here includes the calculations required for both equilibrium and frozen speeds of sound, both of which are important parameters in nonequilibrium flows. The equilibrium speed of sound is a necessary variable in flux splitting numerical techniques for fluid flow, and the improvements in smoothness and continuity of this variable over the best available curve fit data have been pointed out.

12) Acknowledgements.

This work is supported by the joint SERC/MoD grant number GR/F 90035. I would like to thank Prof. B. E. Richards and Dr. F. Watson for their help with the production of this report.

13) References.

1. Anderson, J. M., "Implementation of Equilibrium Air Models Within the Framework of an Existing Euler Code", Department of Aerospace Engineering Report No. 8906, University of Glasgow, 1989.

2. Vincenti, W. G. and Kruger, C. H., "Introduction to Physical Gas Dynamics", Kreiger Publishing Co., 1965.

3. Mayer, J. E. and Mayer, M. G., "Statistical Mechanics", John Wiley & Sons, 1940.

4. Moore, C. E.(ed.), "Atomic Energy Levels", Circular of the National Bureau of Standards, 467, Volume 1, June 1949.

5. Prabhu, R. K. and Erickson, W. D., "A Rapid Method for the Computation of Equilibrium Chemical Composition of Air to 15 000 K", NASA Technical Paper 2792, 1988.

6. Park, C., "Nonequilibrium Hypersonic Aerothermodynamics", John Wiley & Sons, 1990.

7. Poll, D. I. A. and Hodgson, J. P., "The Development of an Equilibrium Gas Code Module for Aerodynamic Design of HOTOL-type Space Vehicles", Department of Engineering, University of Manchester, December 1988.

8. Kuo, K. K., "Principles of Combustion", John Wiley & Sons, 1986.

9. Anderson, W. K., Thomas, J. L. and van Leer, B., "Comparison of Finite Volume Flux Splittings for the Euler Equations", AIAA Paper 85-0122, January 1985.

10. Anderson, J. M., "Implementation of Equilibrium Air Models in Implicit Computational Schemes for the Euler Equations", Department of Aerospace Engineering Report No. 9121, University of Glasgow, 1991.

11. Royal Aeronautical Society, "Mollier Chart of the Thermodynamic Properties of Argon-free Air in Dissociation Equilibrium", Data Sheets 00.01.11 and 00.01.12, June 1962.

12. Fröberg, C-E, "Numerical Mathematics - Theory and Computer Applications", The Benjamin/Cummings Publishing Co., 1985.

13. Srinivasan, S., Tannehill, J. C. and Weilmuenster, K. J., "Simplified Curve Fits for the Thermodynamic Properties of Equilibrium Air", NASA-RP1181, 1987.

14. Tannehill, J. C. and Mugge, P. H., "Improved Curve Fits for the Thermodynamic Properties of Equilibrium Air Suitable for Numerical Computation Using Time-Dependent Shock Capturing Methods", NASA CR-2470, 1974.

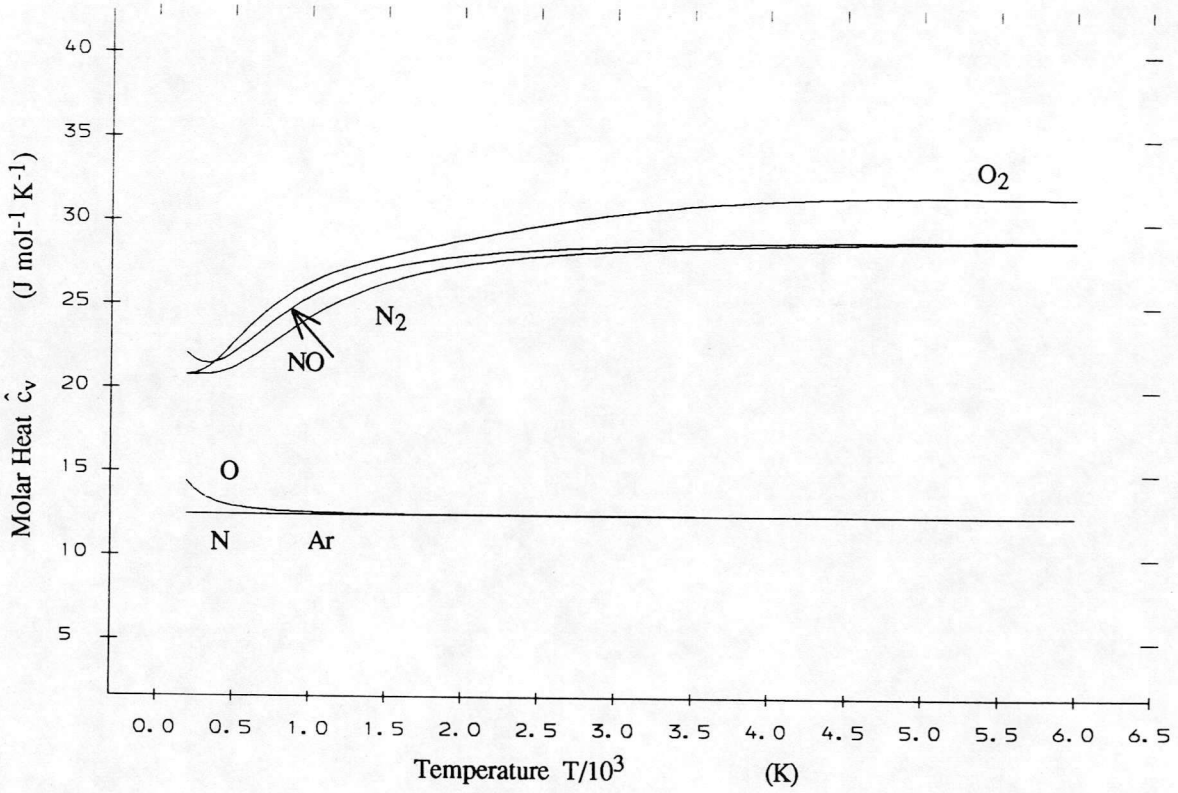

Figure 1) Molar Heat Variation with Temperature Calculated from Simplified Statistical Mechanics Data.

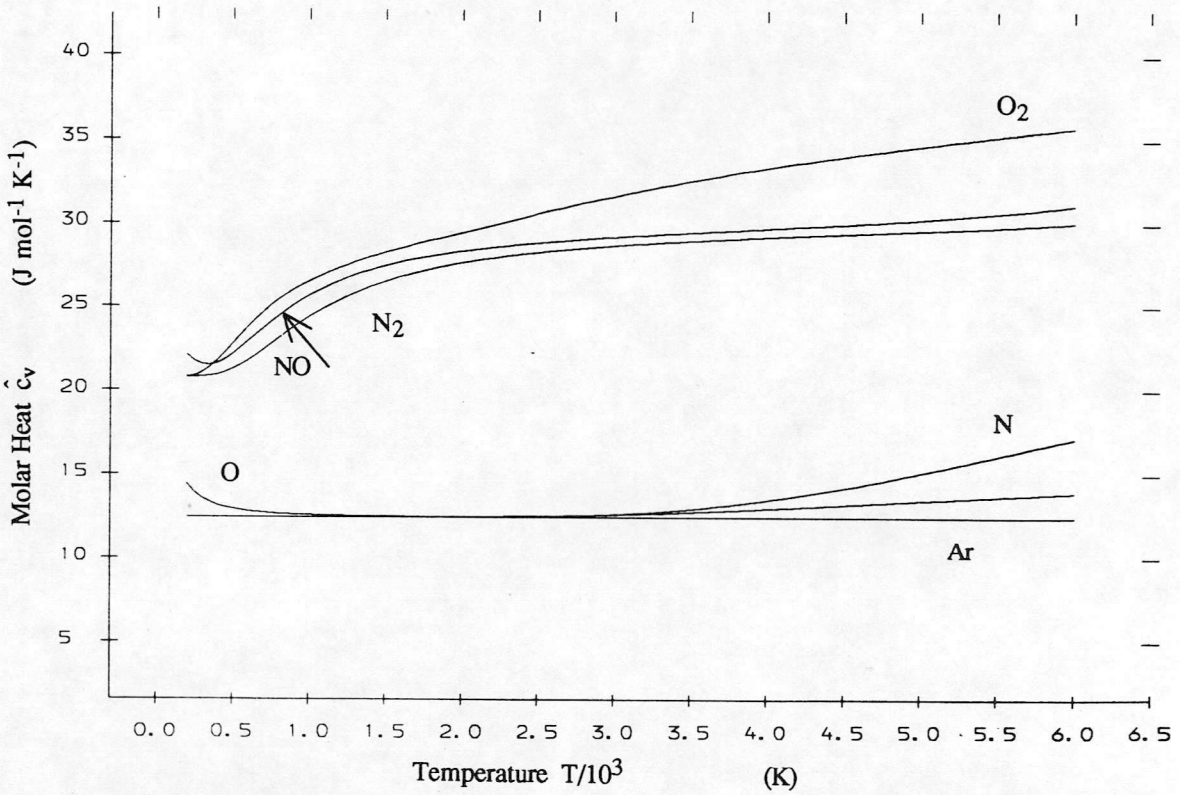

Figure 2) Molar Heat Variation with Temperature Calculated from Curve Fit Data.

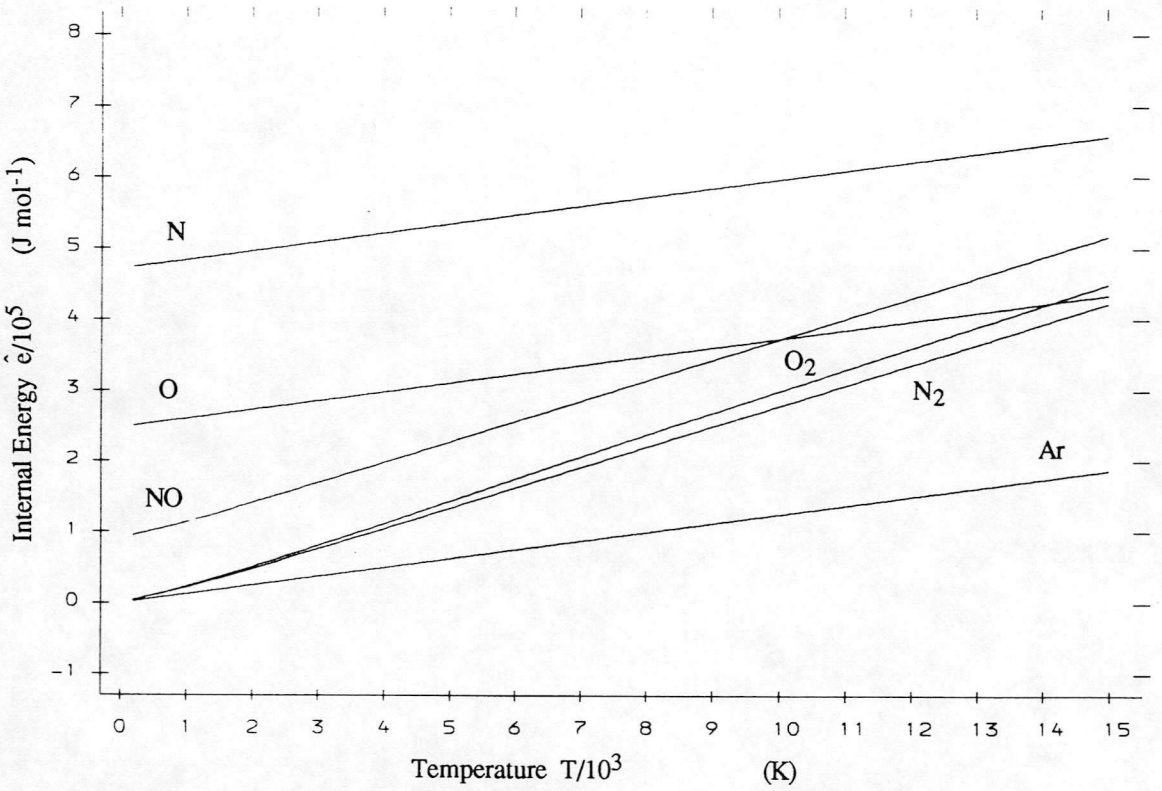

Figure 3) Molar Internal Energy Variation with Temperature Calculated from Simplified Statistical Mechanics Data.

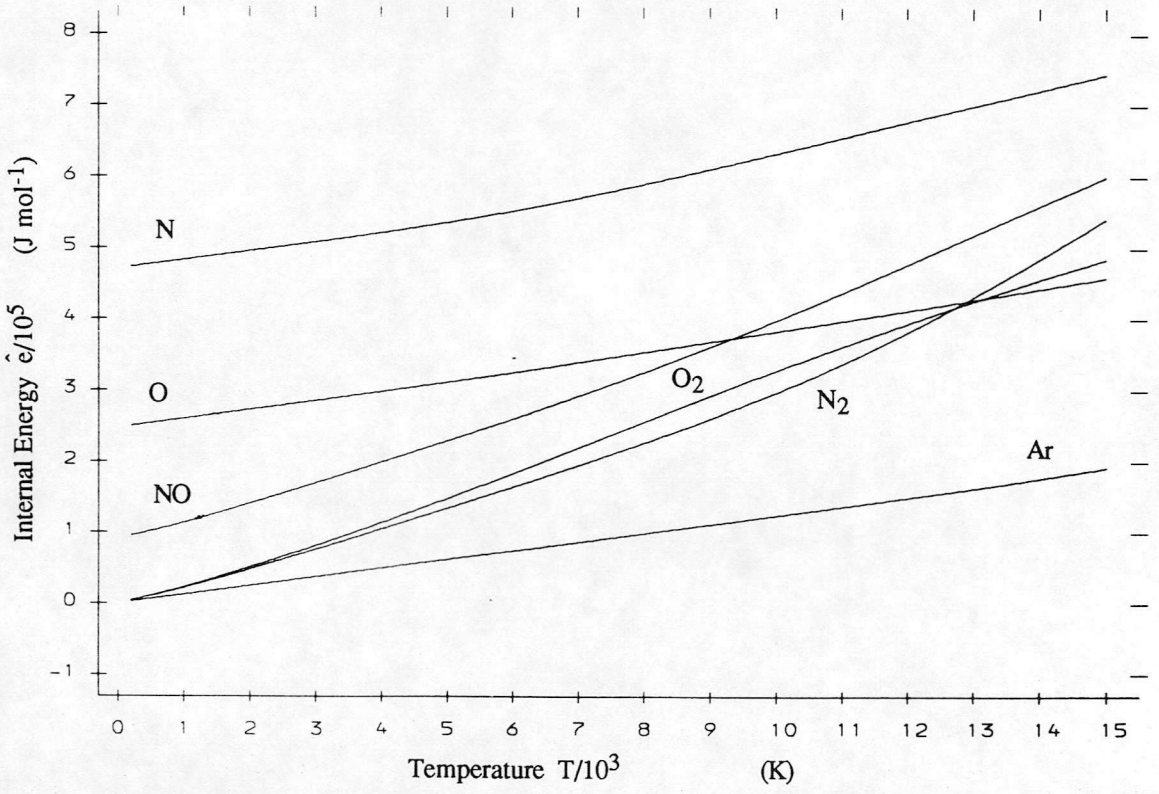

Figure 4) Molar Internal Energy Variation with Temperature Calculated from Curve Fit Data.

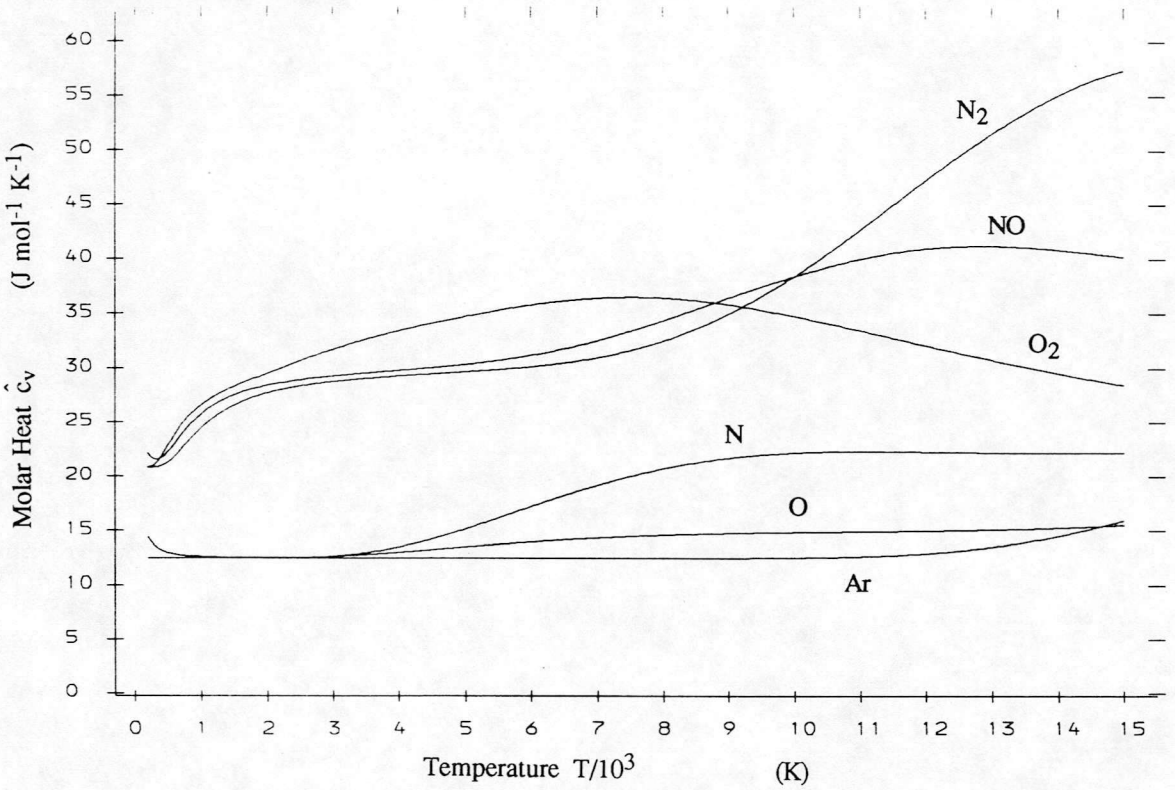

Figure 5) Molar Heat Variation with Temperature Between 200K and 15000K, from Curve Fit Data.

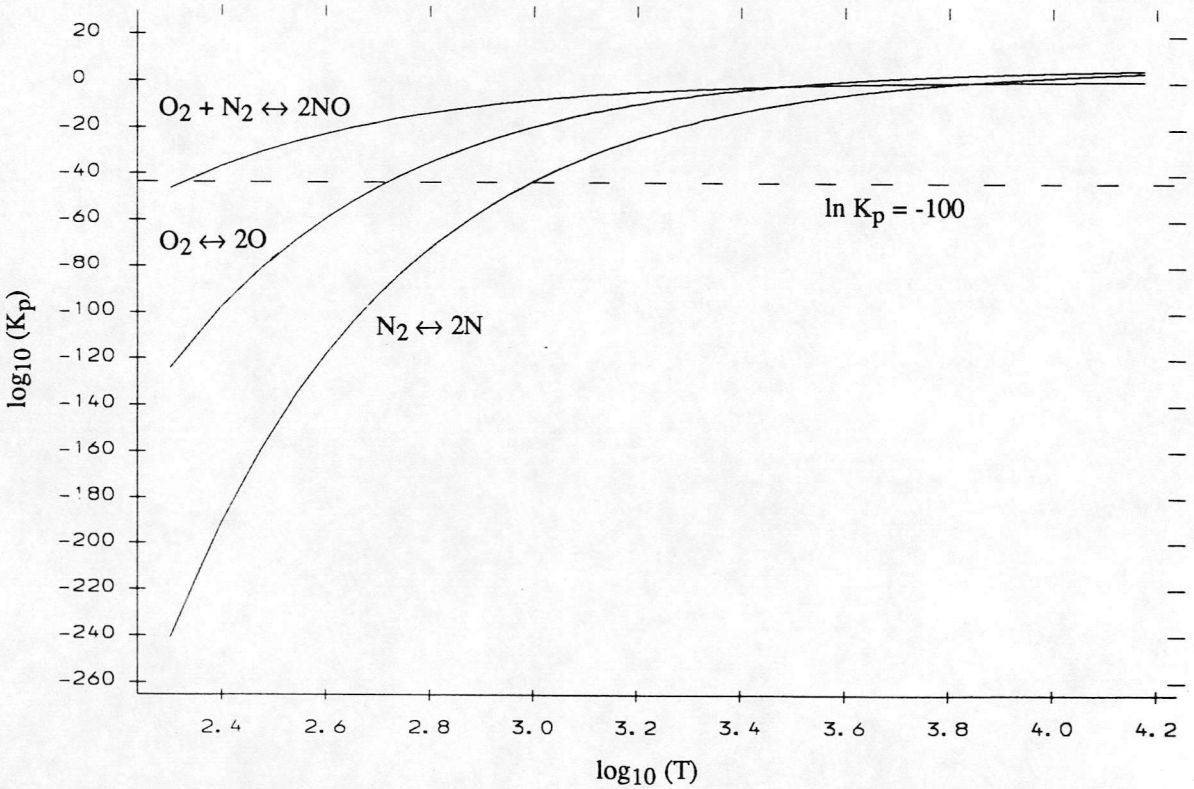

Figure 6) Equilibrium Constants in Terms of Partial Pressures.

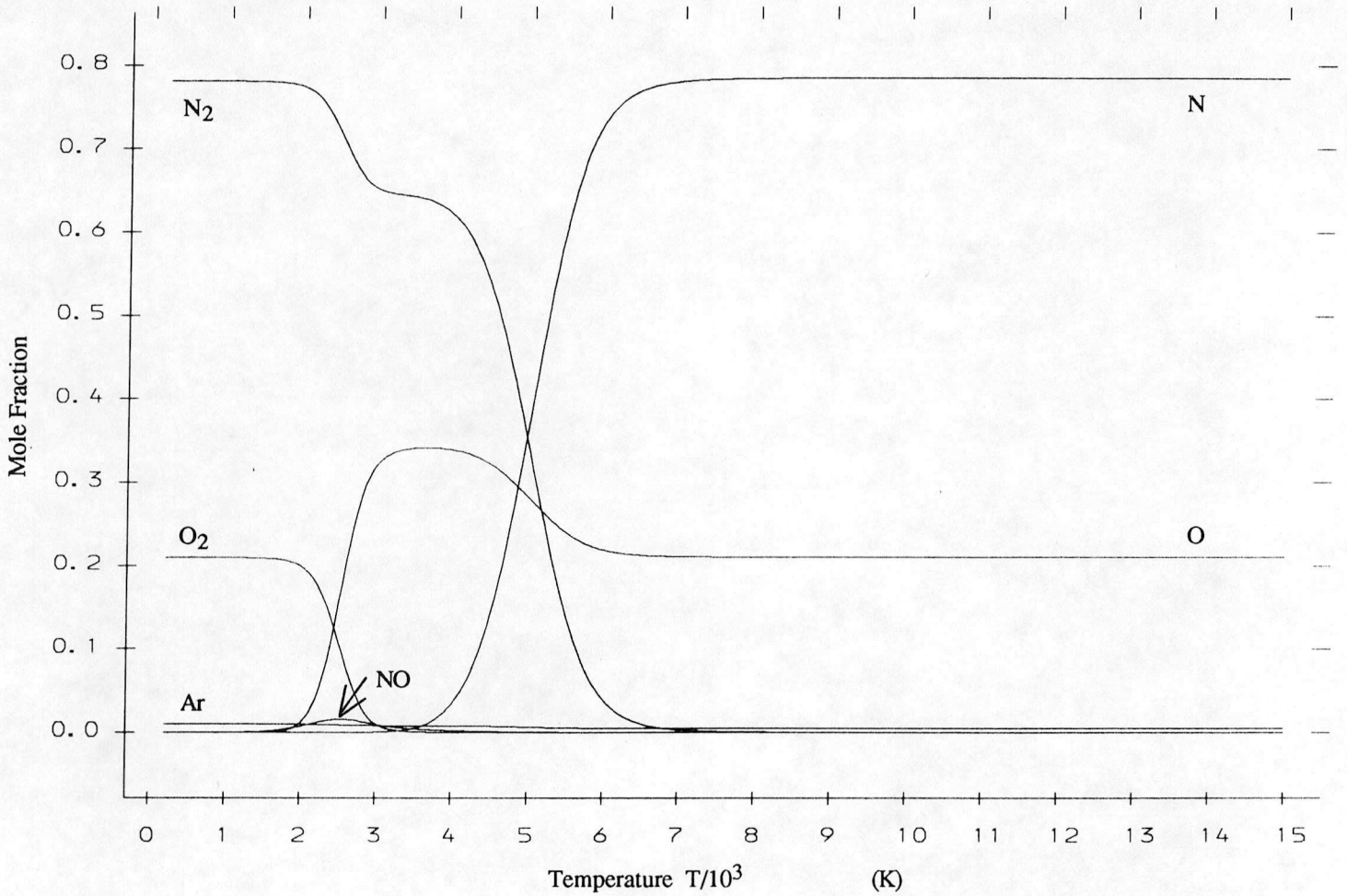

Figure 7) Chemical Composition of Air at 1.225×10^{-4} kg m^{-3}.

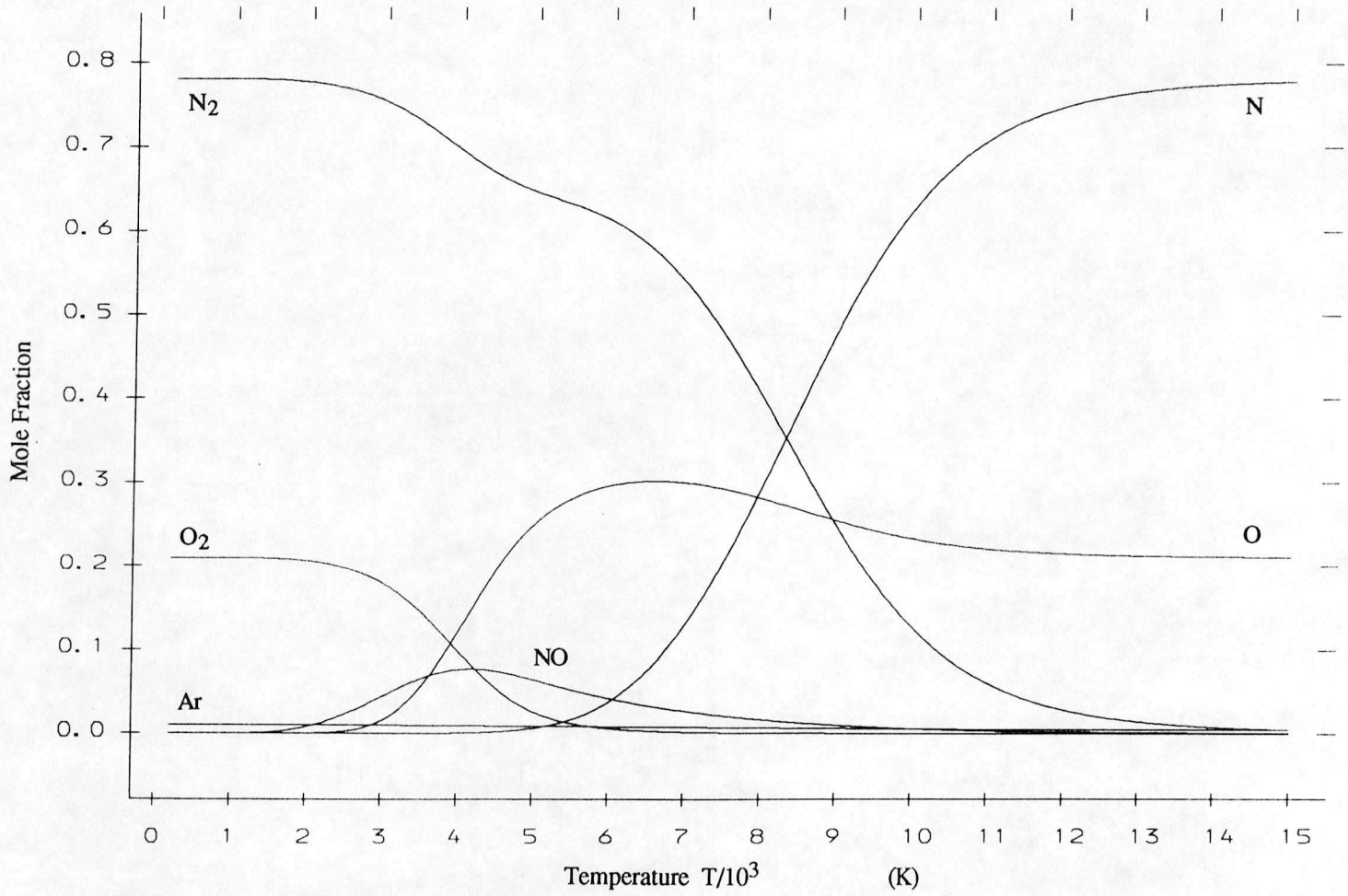

Figure 8) Chemical Composition of Air at 1.225 kg m^{-3}.

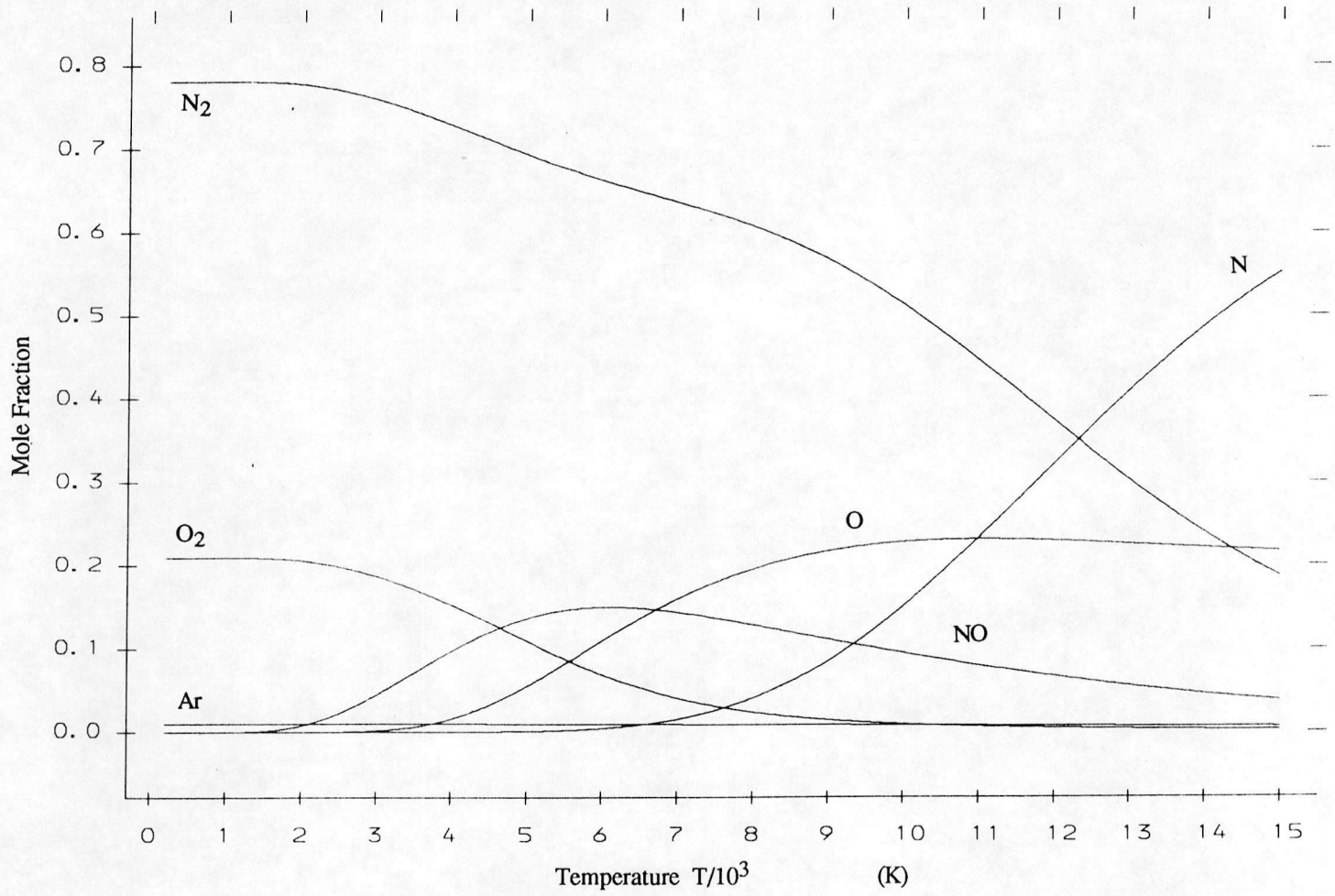

Figure 9) Chemical Composition of Air at 122.5 kg m^{-3}.

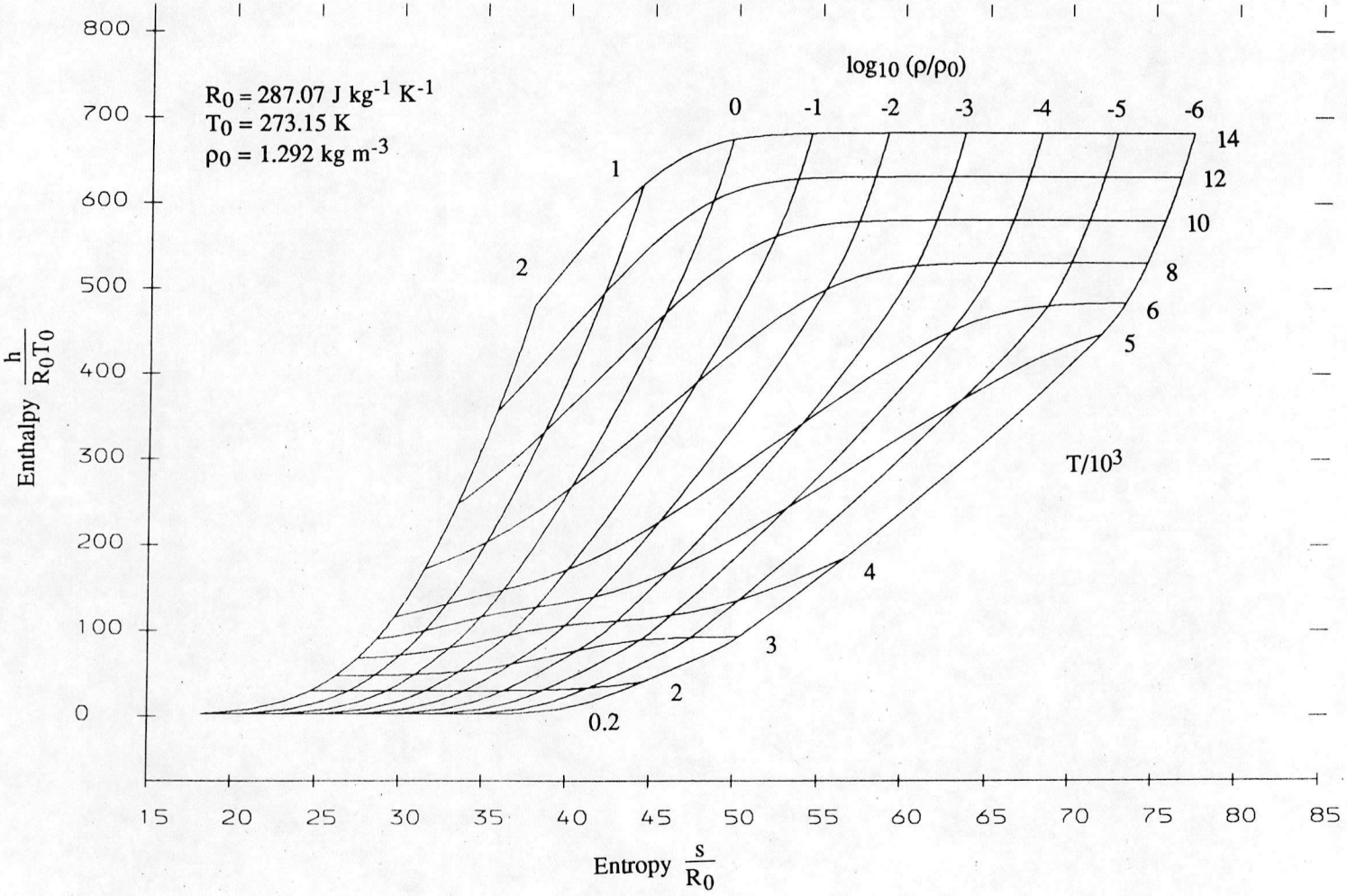

Figure 10) Ehthalpy-Entropy Chart for Constant Density and Temperature.

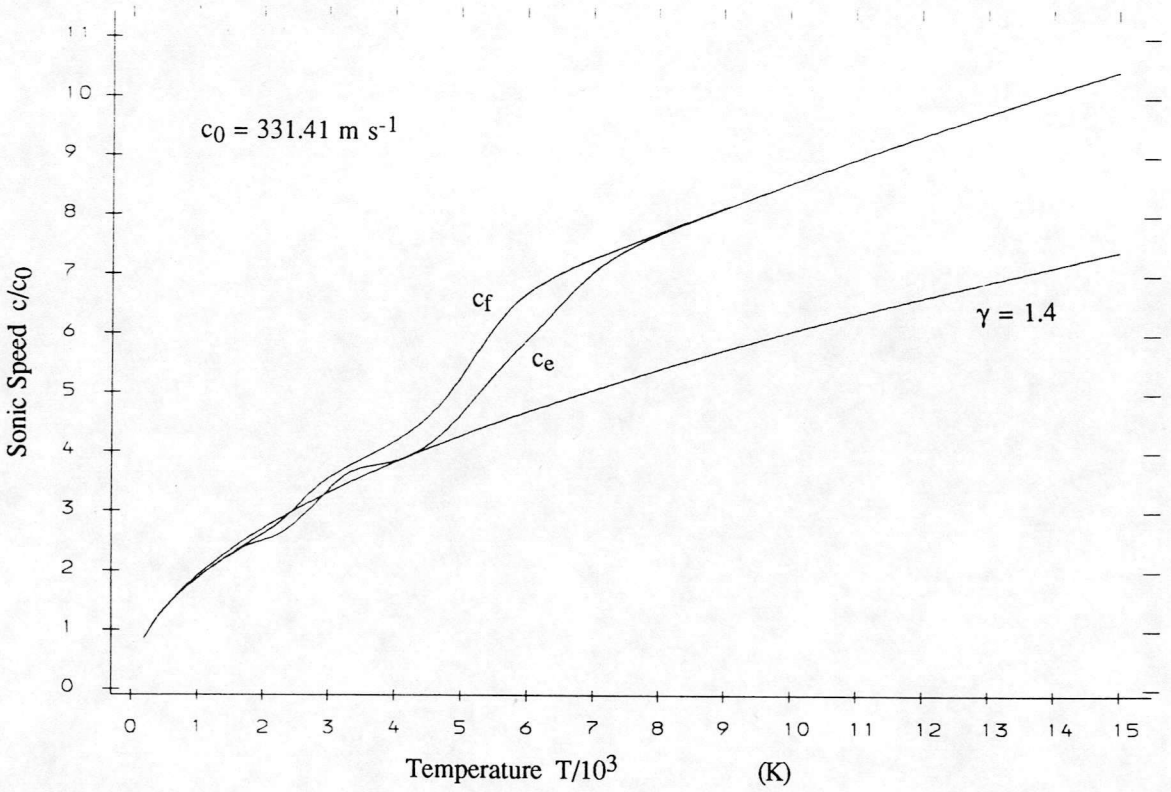

Figure 11) Perfect, Equilibrium and Frozen Speeds of Sound at 1.225 x 10^{-4} kg m^{-3}.

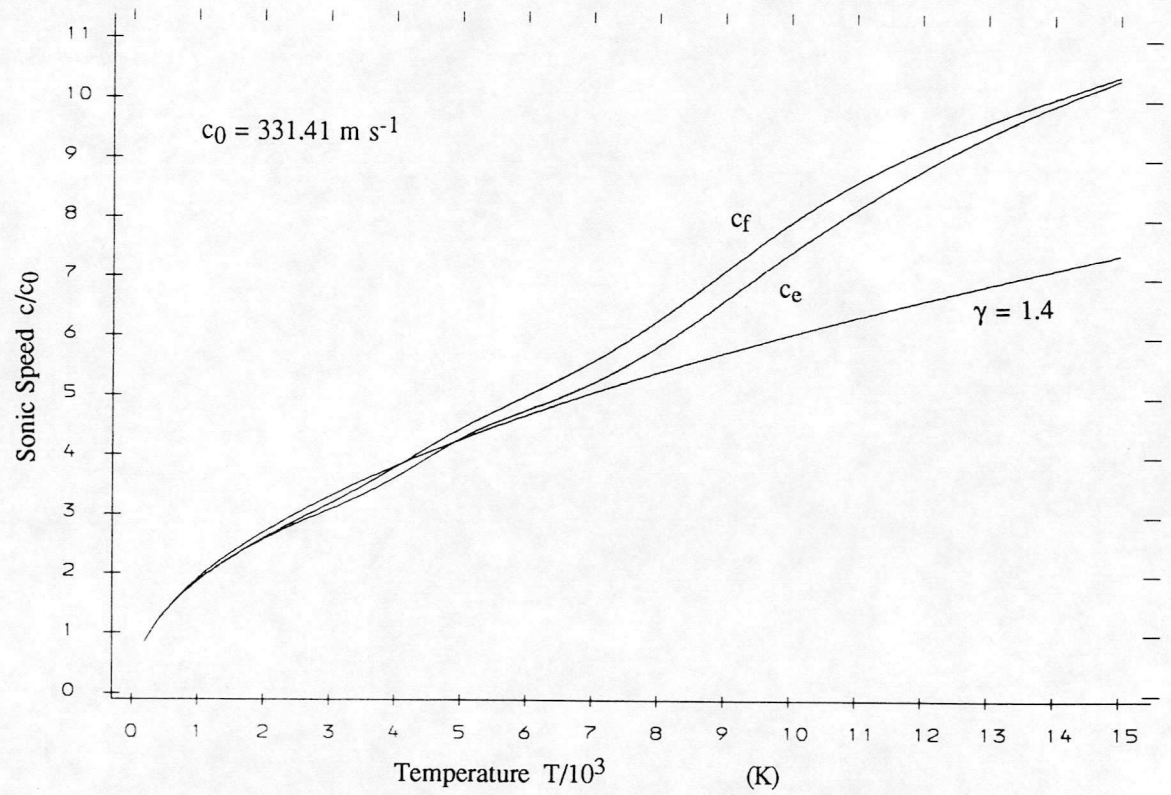

Figure 12) Perfect, Equilibrium and Frozen Speeds of Sound at 1.225 kg m^{-3}.

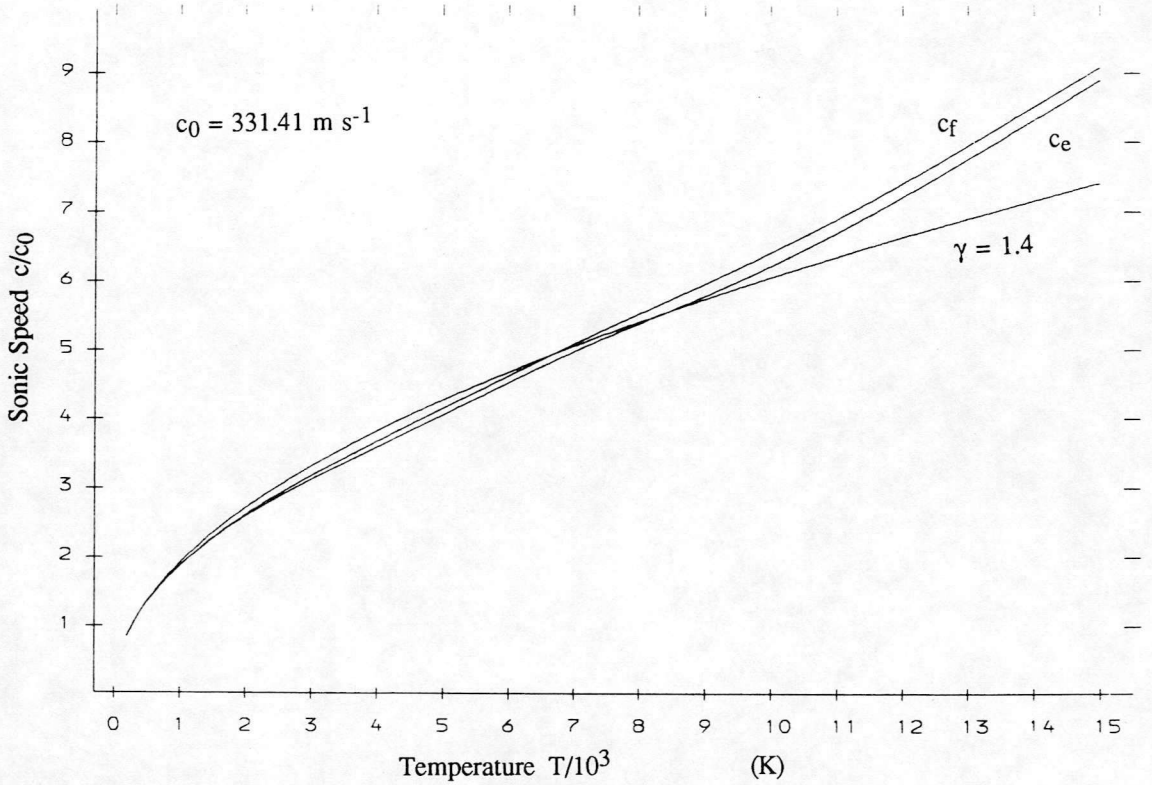

Figure 13) Perfect, Equilibrium and Frozen Speeds of Sound at 122.5 kg m^{-3}.

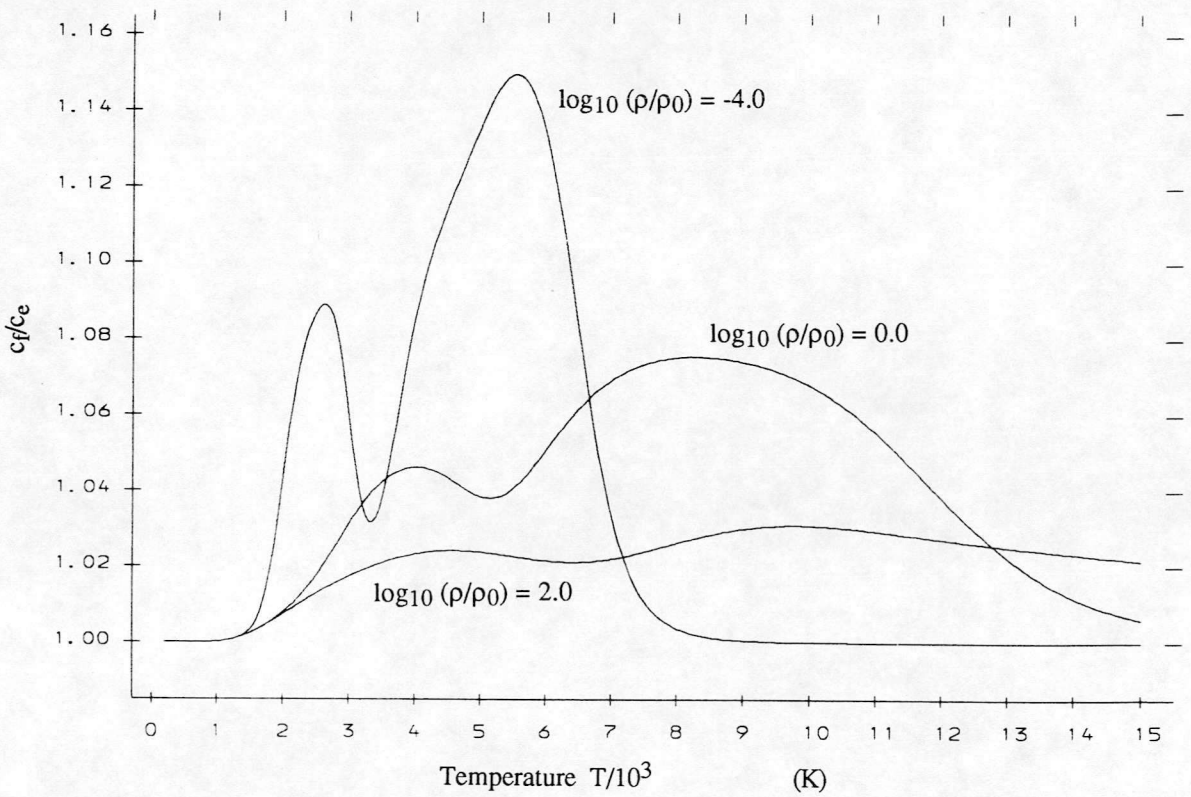

Figure 14) Frozen to Equilibrium Sonic Speed Ratio.

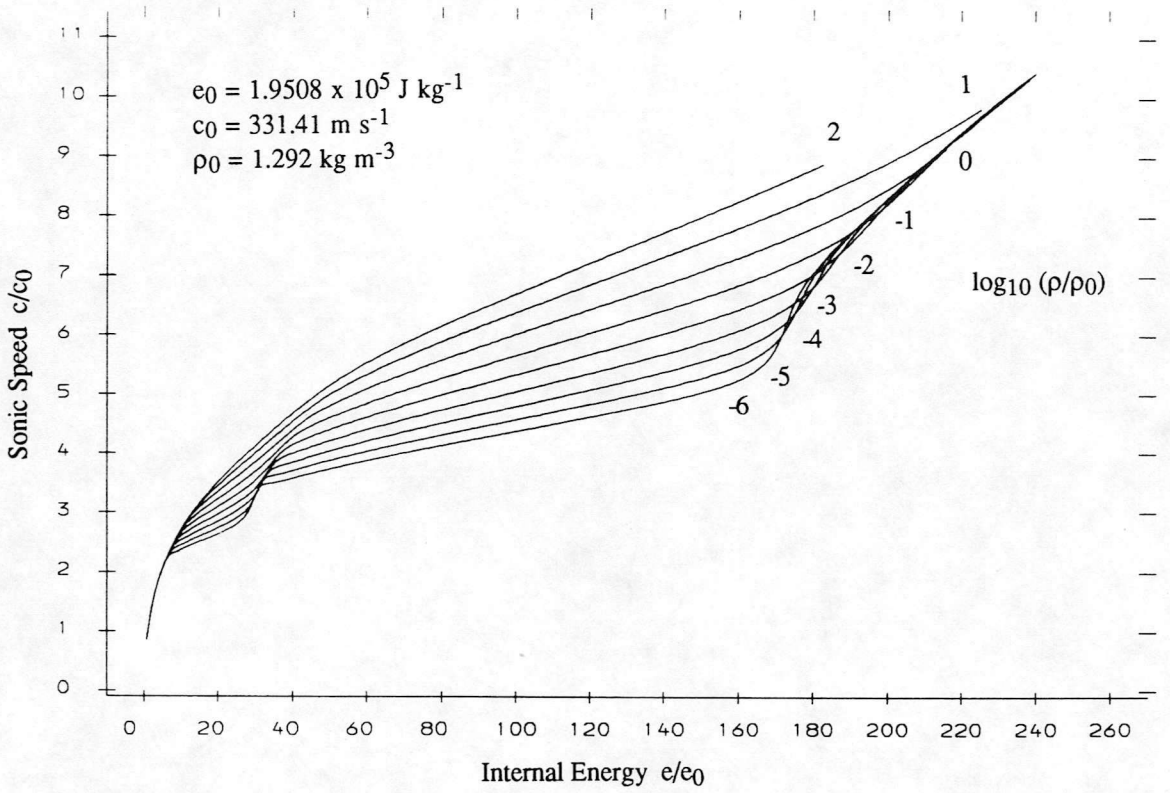

Figure 15) Equilibrium Sonic Speed Variation with Specific Internal Energy.

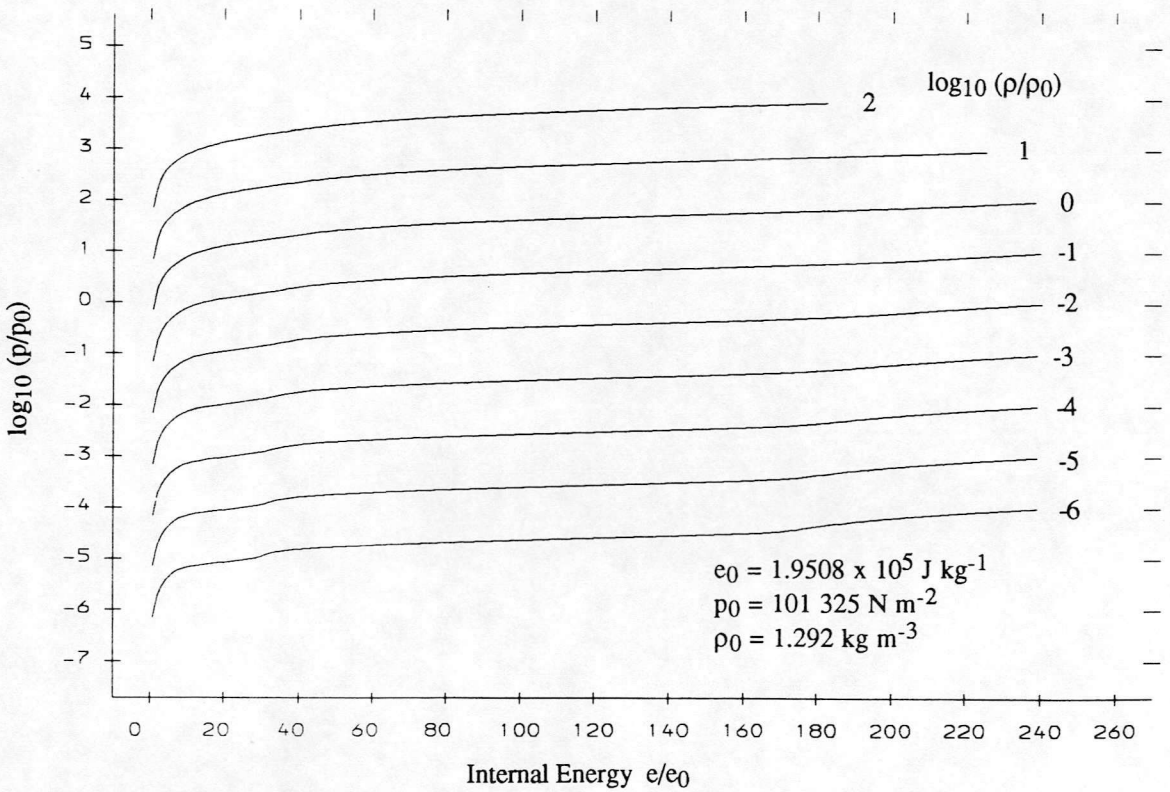

Figure 16) Pressure Variation with Specific Internal Energy.

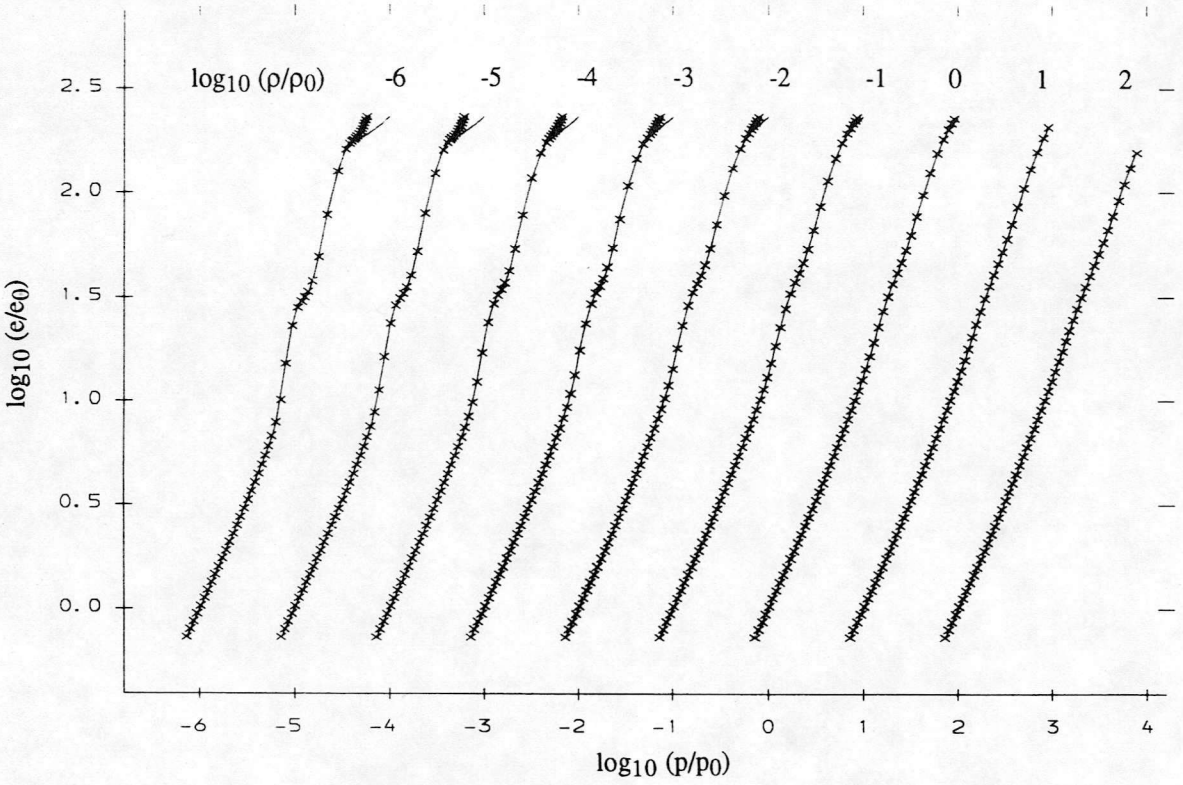

Figure 17) Comparative Results Between Curve Fit Data and Calculated Data for Specific Internal Energy Variation with Pressure.

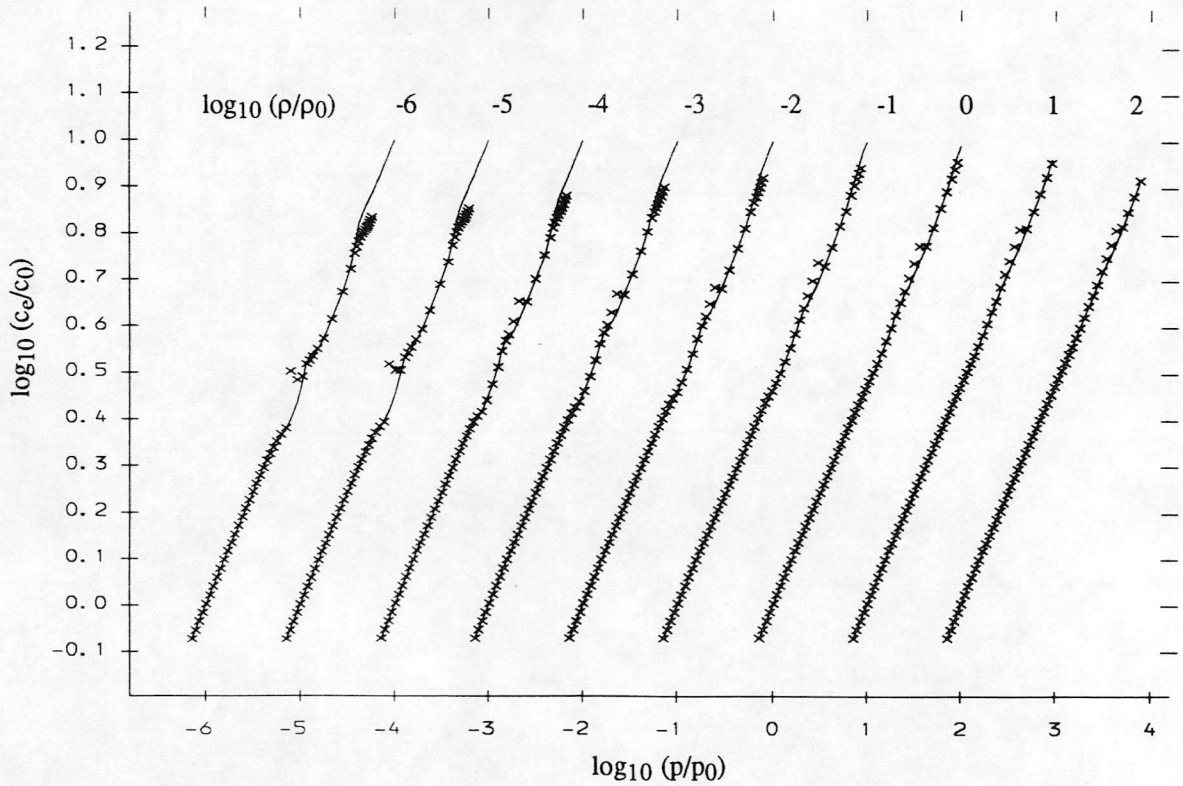

Figure 18) Comparative Results Between Curve Fit Data and Calculated Data for Equilibrium Sonic Speed Variation with Pressure.